AFRL-ML-WP-TR-2000-4099

ADVANCED THERMAL BARRIER COATING

DR. RABI S. BHATTACHARYA

UNIVERSAL ENERGY SYSTEMS, INC.
4401 DAYTON-XENIA ROAD
DAYTON, OH 45432-1894

APRIL 2000

FINAL REPORT FOR 05/03/1999 – 02/03/2000

THIS IS A SMALL BUSINESS INNOVATION RESEARCH (SBIR) PHASE I REPORT.

MATERIALS AND MANUFACTURING DIRECTORATE
AIR FORCE RESEARCH LABORATORY
AIR FORCE MATERIEL COMMAND
WRIGHT-PATTERSON AIR FORCE BASE OH 45433-7750

NOTICE

WHEN GOVERNMENT DRAWINGS, SPECIFICATIONS, OR OTHER DATA ARE USED FOR ANY PURPOSE OTHER THAN IN CONNECTION WITH A DEFINITELY GOVERNMENT-RELATED PROCUREMENT, THE UNITED STATES GOVERNMENT INCURS NO RESPONSIBILITY OR ANY OBLIGATION WHATSOEVER. THE FACT THAT THE GOVERNMENT MAY HAVE FORMULATED OR IN ANY WAY SUPPLIED THE SAID DRAWINGS, SPECIFICATIONS, OR OTHER DATA, IS NOT TO BE REGARDED BY IMPLICATION OR OTHERWISE IN ANY MANNER CONSTRUED, AS LICENSING THE HOLDER OR ANY OTHER PERSON OR CORPORATION, OR AS CONVEYING ANY RIGHTS OR PERMISSION TO MANUFACTURE, USE, OR SELL ANY PATENTED INVENTION THAT MAY IN ANY WAY BE RELATED THERETO.

THIS REPORT IS RELEASABLE TO THE NATIONAL TECHNICAL INFORMATION SERVICE (NTIS). AT NTIS, IT WILL BE AVAILABLE TO THE GENERAL PUBLIC, INCLUDING FOREIGN NATIONS.

THIS TECHNICAL REPORT HAS BEEN REVIEWED AND IS APPROVED FOR PUBLICATION.

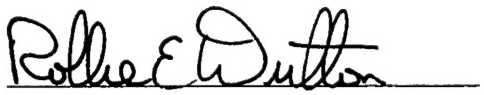

ROLLIE E. DUTTON
Metals Development & Materials
Processing Branch
Metals, Ceramics & NDE Division

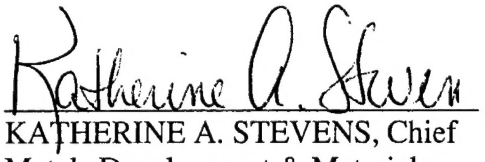

KATHERINE A. STEVENS, Chief
Metals Development & Materials
Processing Branch
Metals, Ceramics & NDE Division

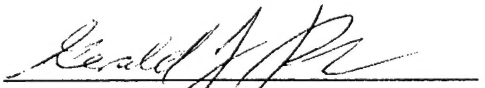

GERALD J. PETRAK, Asst Chief
Metals, Ceramics & NDE Division
Materials & Manufacturing Directorate

IF YOUR ADDRESS HAS CHANGED, IF YOU WISH TO BE REMOVED FROM OUR MAILING LIST, OR IF THE ADDRESSEE IS NO LONGER EMPLOYED BY YOUR ORGANIZATION, PLEASE NOTIFY, AFRL/MLLM, WRIGHT-PATTERSON AFB OH 45433-7817 TO HELP US MAINTAIN A CURRENT MAILING LIST.

COPIES OF THIS REPORT SHOULD NOT BE RETURNED UNLESS RETURN IS REQUIRED BY SECURITY CONSIDERATIONS, CONTRACTUAL OBLIGATIONS, OR NOTICE ON A SPECIFIC DOCUMENT.

REPORT DOCUMENTATION PAGE	Form Approved OMB No. 0704-0188

1. AGENCY USE ONLY *(Leave blank)*	2. REPORT DATE	3. REPORT TYPE AND DATES COVERED
	APRIL 2000	FINAL REPORT FOR 05/03/1999 - 02/03/2000

4. TITLE AND SUBTITLE
ADVANCED THERMAL BARRIER COATING

5. FUNDING NUMBERS
C F33615-99-C-5206
PE 65502
PR 3005
TA ML
WU 09

6. AUTHOR(S)
DR. RABI S. BHATTACHARYA

7. PERFORMING ORGANIZATION NAME(S) AND ADDRESS(ES)
UNIVERSAL ENERGY SYSTEMS, INC.
4401 DAYTON-XENIA ROAD
DAYTON, OH 45432-1894

8. PERFORMING ORGANIZATION REPORT NUMBER

9. SPONSORING/MONITORING AGENCY NAME(S) AND ADDRESS(ES)
MATERIALS AND MANUFACTURING DIRECTORATE
AIR FORCE RESEARCH LABORATORY
AIR FORCE MATERIEL COMMAND
WRIGHT-PATTERSON AFB, OH 45433-7750
POC: ROLLIE E. DUTTON, AFRL/MLLM, 937-255-9396

10. SPONSORING/MONITORING AGENCY REPORT NUMBER
AFRL-ML-WP-TR-2000-4099

11. SUPPLEMENTARY NOTES
THIS IS A SMALL BUSINESS INNOVATION RESEARCH (SBIR) PHASE I REPORT.

12a. DISTRIBUTION AVAILABILITY STATEMENT
APPROVE FOR PUBLIC RELEASE, DISTRIBUTION UNLIMITED.

12b. DISTRIBUTION CODE

13. ABSTRACT *(Maximum 200 words)*

This report was developed under SBIR contract for topic AF99-148.

The primary research objective of this work was to develop a novel thermal barrier coating (TBC) system by depositing a high quality alpha alumina sublayer on the metallic bond-coat, prior to the deposition of the yttria stabilized zirconia (YSZ) coating. A patented filtered cathodic arc deposition equipment was used to deposit an alpha alumina layer on a superalloy that was plasma-spray coated with a NiCoCrAlY bond-coat. The filtered arc coating process allows droplet-free deposition of coatings. Also, this process provides high ionization (>90%) compared with the standard physical vapor deposition processes (<20%), thereby providing excellent bonding between the coating and the substrate. Using this approach, 0.5-0.6 micron thick alpha alumina coatings were deposited on metallic substrate at 925°C. Oxidation tests reveal that further improvements are necessary for the system to perform better than state-of-the-art TBCs. The performance was impaired by microstructural instability and surface rumpling of the bond-coat, which caused failure of the alumina layer at a number of locations.

14. SUBJECT TERMS	15. NUMBER OF PAGES
SBIR Report, Thermal Barrier Coating, Alumina Coating, Alpha Alumina, Filtered Cathodic Arc, Physical Vapor Deposition, Yttria Stabilized Zirconia, Turbine Engine, TBC, Oxidation.	35
	16. PRICE CODE

17. SECURITY CLASSIFICATION OF REPORT	18. SECURITY CLASSIFICATION OF THIS PAGE	19. SECURITY CLASSIFICATION OF ABSTRACT	20. LIMITATION OF ABSTRACT
UNCLASSIFIED	UNCLASSIFIED	UNCLASSIFIED	SAR

PREFACE

This technical report has been prepared as part of the requirement of the Phase I SBIR Contract No. F33615-99-C-5206 with the Air Force Research Laboratory/MLLM, Wright-Patterson Air Force Base, Ohio. The report covers work conducted during the period 3 May 1999 through 3 February 2000, and constitutes the final report under this contract. The Air Force Project Engineers were Dr. Rollie E. Dutton and Dr. Edmund Moore.

ACKNOWLEDGEMENT

The author wishes to acknowledge the support of Dr. Bhaskar S. Majumdar, New Mexico Institute of Technology, Department of Materials and Metallurgical Engineering, as a subcontractor. He was the Principal Investigator of this project prior to his departure for his new position. He has performed most of the oxidation tests and part of the characterizations in this project, and also helped in the preparation of this report. Mr. Boris Brodkin and Dr. A.K. Rai of UES have performed coating deposition and characterization, respectively.

1.0 INTRODUCTION

Thermal Barrier Coatings (TBCs) are used in the hot section of aircraft engine turbines to increase turbine efficiency and to extend the life of metal components.

1.1 ADVANTAGES OF THERMAL BARRIER COATINGS AND THEIR CURRENT LIMITATIONS

The advantages of thermal barrier coatings (TBCs) in hot-section turbine components are best illustrated by Figure 1.

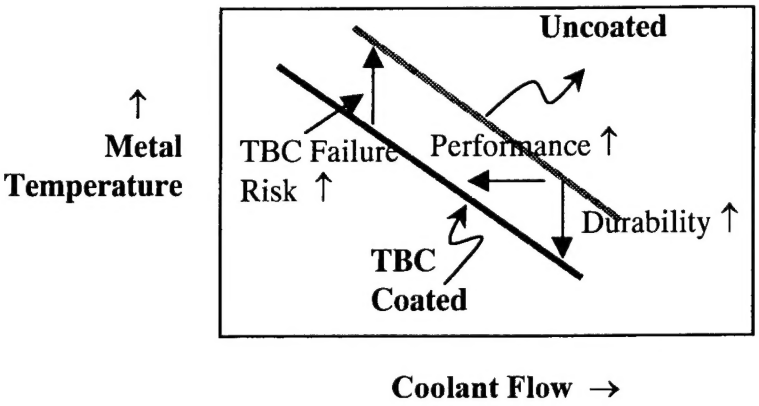

Figure 1. Advantages and risks associated with TBCs as compared to uncoated metal under exposure to the same temperature environment.

The main advantages of the TBC are:

(i) At constant coolant flow, they reduce the base metal temperature, thereby increasing the life of that part. Advanced turbine blades in aerospace engines operate very close to their melting temperature, and it is estimated that a 15°C reduction in metal temperature can produce a two-fold increase in life [1-3].

(ii) At existing metal temperature, the temperature at the TBC surface can be increased by as much as 65°C, leading to a substantial gain in fuel efficiency. It is estimated that this temperature advantage is equivalent to two generations of new superalloy development [1-3].

These advantages constitute immense cost savings to the Air Force and the Navy. Unfortunately, the above benefits of TBCs have not been realized in practice. This is largely because the performance of even the advanced TBCs is not considered sufficiently reliable and predictable [4] (i.e., the risk factor illustrated in Figure 1). In addition, the life of these TBCs need significant improvement. In military engines that employ state-of-the-art single crystal blades such as those fabricated from PW1480 or Rene N5, the maximum temperatures are in the neighborhood of 1150°C. The typical life of the most advanced TBC for a 23°C – 1150°C temperature cycle ranges between 200 and 500 cycles, and in addition there is the problem of reliability.

Turbine blades in commercial aircraft experience lower temperatures. Cost considerations do not favor the use of single crystal or directionally solidified blades in most instances. Also, while chemistry control is strictly adhered to, the levels of allowable impurities in the blade may be larger, since the operating conditions are less severe. At the same time, however, the significantly higher risks associated

with TBC failure, and the requirement that it provides much longer life than in military engines, stipulates that TBC performance will be even more critically examined in commercial engines.

Thus, there is a need to develop TBC systems that have significantly higher reliability and durability than current state-of-the-art systems.

1.2 MECHANISMS AND MECHANICS OF FAILURE OF TBCs

We illustrate the four essential components of a TBC system in Figure 2. The base superalloy substrate is normally vacuum plasma spray (VPS) coated with a bond-coat such as MCrAlY (where M is either Ni, Co, or both) or a complex Pt-based aluminide of typical thickness 75-100 μm. Upon this layer is deposited a 6-8 wt.% yttria stabilized zirconia (YSZ) layer of approximately 100 μm thickness. The YSZ is typically applied either by a plasma spray process or by electron beam physical vapor deposition (EB PVD). The plasma spray deposited YSZ contains many pores and defects that constitute crack nucleation sites, and failure in this system typically initiates in the YSZ close to the metal substrate. The life of plasma sprayed YSZ is generally much lower than YSZ deposited by EB PVD, and hence was not considered in this work. The advantages of EB PVD deposited YSZ are its superior quality, and a columnar morphology that leads to significant increase in coating compliance and hence lower YSZ stresses.

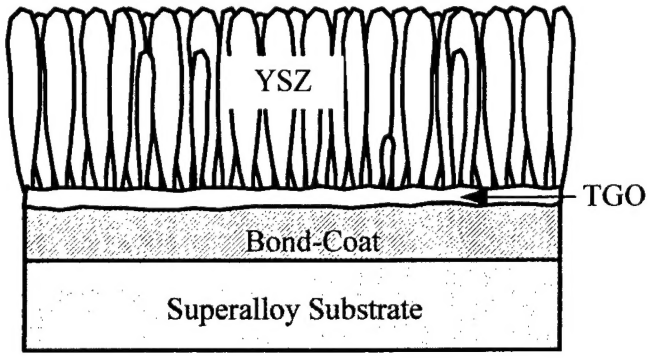

Figure 2. Sketch illustrating the primary components of a traditional thermal barrier coating.

Upon exposure to air at high temperatures, an oxide layer forms at the interface between the bond-coat and the YSZ [1,5]. This is called the thermally grown oxide (TGO) layer, whose growth is aided by the columnar morphology of the YSZ that allows easy penetration of oxygen. While the TGO is largely composed of alpha alumina, which is the most stable phase, it can also contain substantial amounts of mixed oxides, such as spinels of the type Ni $(Cr,Al)_2O_4$, or Cr_2O_3, etc. [6-8]. The TGO is a non-equilibrium region, and grows in the presence of oxygen that is continuously fed by the open channel YSZ layer. The typical thickness of TGO after thermal exposure is reported to be about 5 μm [9-11].

The failure mechanism of the TBC is intimately connected with the formation and growth of the TGO. During the initial stages of oxidation, blister type spots can be observed on the TBC surface by thermal wave imaging, or even optically if the blisters are quite large. At a later stage, these blisters either combine, or a single one grows to such a point that a piece of the YSZ layer detaches from the blade. The exact mechanics depend on the system under consideration, and Figure 3 provides a plausible picture of the progression of damage. Microcracks initially form in the TGO and often tend to propagate along the bond-coat/TGO interface [3,4,9,12]. Continued oxidation and opening of these cracks initiate bulges that manifest as surface irregularities on the YSZ outer surface. At this point, two scenarios can operate: (i) either the interface crack kinks into the YSZ ceramic, leading to its cracking and separation (Figure 3c), or (ii) there is buckling induced delamination of the YSZ, because of compressive stresses in

the TGO and the YSZ layer (Figure 3d). The former case does not require the formation of a buckle, but is driven by a greater kink instability with increasing Mode II mixity as the delamination size grows. In the latter case, the bending stresses associated with buckle formation ultimately leads to crack kinking into the YSZ, and this is believed to be the primary spallation mechanism.

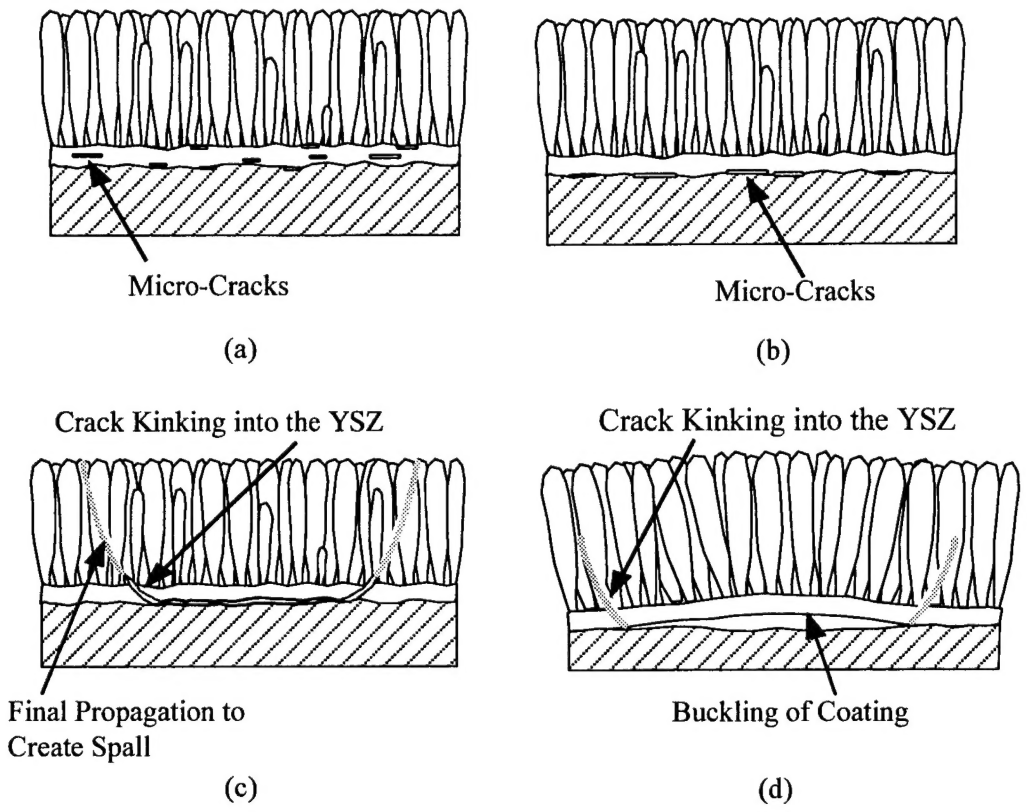

Figure 3. Plausible damage progression in traditional thermal barrier coatings. Micro-cracks initially nucleate either in the TGO (a), or at the TGO/bond-coat interface (b). These grow and coalesce to form larger interface cracks. These cracks can then either kink into the TBC by an instability mechanism (c), or it can buckle when the crack length becomes larger (d). The latter also finally gives rise to a kinked crack. The current understanding is that spallation is largely a result of TBC buckling and crack kinking.

Stress analysis on Figure 2 indicates that the TGO layer is under very high in-plane compressive residual stress at room temperature; a value of 3 GPa is typical [11]. This is because of the significant thermal expansion mismatch between the Ni-base alloy (~$12x10^{-6}$/C) and the alumina (~$8x10^{-6}$/C). If the YSZ layer was not present, and at modest levels of fracture toughness of the TGO/bond-coat interface, this level of compressive stress in conjunction with a micro defect can be sufficient to a buckling induced delamination failure of the TGO. The presence of the relatively thick YSZ along with its associated stiffness prevents this from happening, unless the crack length becomes large, as will be illustrated presently. Consequently, the initiation of the microcrack requires an explanation as to how an out-of-plane normal stress is generated either within or at the interface of the TGO.

One postulated source for the microcrack formation is heterogeneous volumetric change associated with oxidation of the NiCrAlY bond-coat (Figure 4a). This scenario requires volumetric expansion that has yet to be quantified. A second and more quantifiable mechanism is the presence of

ripples in the TGO (Figure 4b). At the start of our Phase I program, we had assumed it to be caused either by an initially rough bond-coat surface or an uneven oxidation of the bond-coat. The results of the current program suggest that instabilities in the bond-coat microstructures, and thermal expansion difference between the bond-coat and the superalloy substrate, likely play an even larger role. Those will be amplified in a later section. Figure 5 illustrates results from a finite element method (FEM) analysis with a sinusoidal alumina/YSZ interface [12]. The YSZ layer is on the right, and the TGO is on the left side of the figure. The contour region marked A, at the bond-coat/TGO interface, has an out-of-plane stress (i.e., directed to the right of the figure) of approximately 450 MPa. Thus, fairly large out-of-plane stresses can be generated by interface waviness, enough to nucleate delamination cracks at the interface.

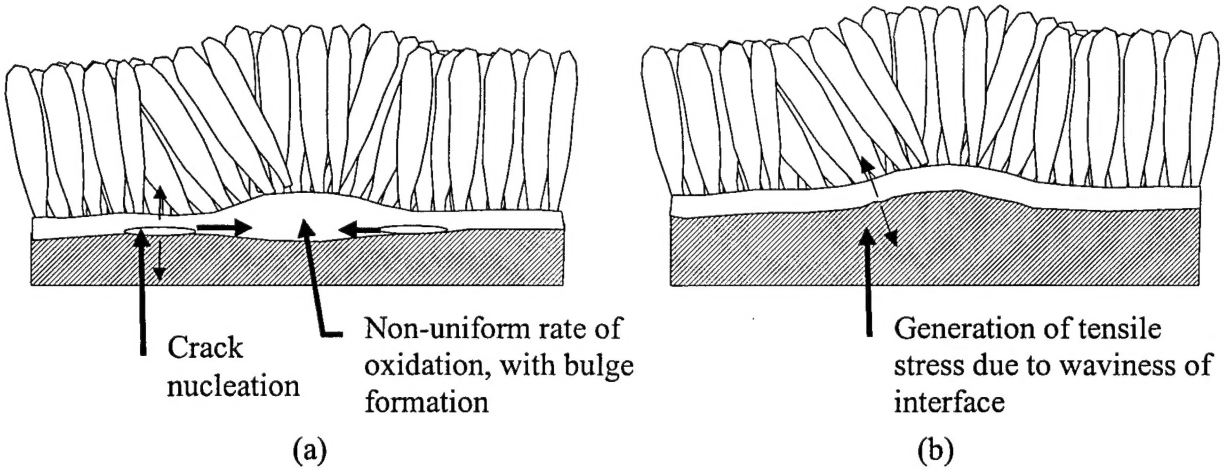

Figure 4. Mechanisms for crack nucleation in the TGO or at the interface. (a) Heterogeneous oxidation can create a bulge and give rise to normal stresses, thereby nucleating cracks that can then proceed towards the bulge. (b) Non-planar bond-coat deposition or non-uniform oxidation can create surface ripples, which cause generation of out-of-plane tensile stresses.

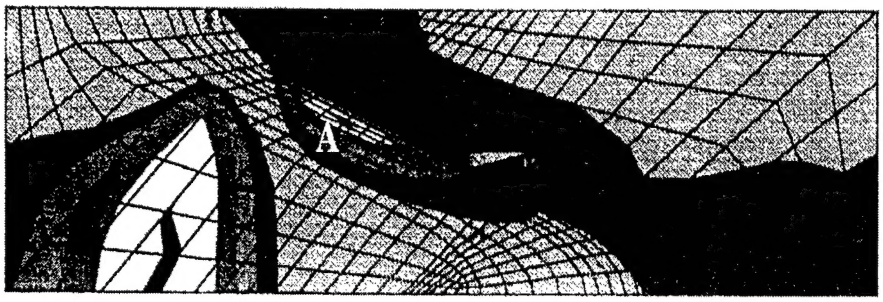

Figure 5. Contour plot from our FEM analysis with a wavy TGO structure. The YSZ layer is on the right, and the bond-coat is on the left. Significant out-of-plane tensile stresses (i.e., along the horizontal axis in the figure) are generated in the small island A (bright) at the bond-coat/TGO interface.

In the case of the diffusion aluminide Pt-Al bond-coat system, the ripple effect is less evident. Rather, large thermal ridges have been observed, occupying as much as 10 to 20% of the bond-coat surface. In this case, cracking of the TGO is observed to occur at these ridges [13]. While stress concentrations do occur in such grooves, some related oxidation studies of aluminide coatings suggest that segregation effects in the grain boundaries can also play a dominant role in enhancing such TGO damage.

The mechanics of buckling induced YSZ spallation has also been probed [12]. In the absence of any interface crack, the critical stress for buckling of the YSZ is approximately 9 GPa, whereas the actual in-plane compressive stress in the YSZ is only about 150 MPa. Clearly, an interface crack, or a crack in the TGO, has to be present for buckling induced spallation of the YSZ to occur.

When an interface crack, or a crack in the TGO layer is already present, the critical stress (σ_c) in the YSZ layer to cause buckling induced spallation is approximately given by: $\sigma_c = (Ec/12).(\pi h/a)^2$, where a is the radius of the delamination crack, h is the coating thickness, and Ec is an effective modulus. *Assuming a YSZ thickness of 0.127 mm, the critical delamination crack radius to cause buckling induced spallation is approximately 1.7 mm, which is a little more than ten times the YSZ thickness. Thus, the interface crack has to grow by a substantial amount before buckling, so that methods that prevent delamination crack growth will be beneficial to TBC life.* In this calculation, it is assumed that Ec at RT is 28 GPa, and the computed residual stress in the YSZ is 140 MPa.

The fracture analyses show that buckling will be delayed by a smaller delamination crack length, lower compressive stress in the YSZ, greater toughness of the YSZ, and a greater thickness of the YSZ. While an increased thickness of the YSZ has the undesirable effect of increasing the delamination crack driving force (which is proportional to YSZ thickness), *it turns out that the compressive energy in the very thin TGO is actually 5 to 10 times larger than in the YSZ, because of the significantly larger stress in the TGO compared with the YSZ. In other words, it is the TGO characteristics that control delamination behavior.*

The stress analyses also indicates that it is extremely important to prevent the formation and initial growth of microcracks in the TGO (or at its interface with either the bond-coat or YSZ). Larger thickness of the TGO aids in microcrack damage, because of the additional defect sites involved (a volume effect), as well as the high compressive energy that is available to drive the growth of incipient cracks in the TGO (energy $\sim\sigma^2 t/E$, where t is TGO thickness, and σ is approximately 3-4 GPa). Typical TGO thickness after thermal cycling is about 5 μm and larger. Clearly, oxidation has to be drastically reduced.

2.0 PHASE I APPROACH

UES, Inc.'s Phase I approach is illustrated in Figure 6. **The most important component of the research was to develop a TBC system that comprised an alpha alumina sublayer, deposited by a novel filtered cathodic arc deposition system.** The standard yttrium stabilized zirconia (YSZ) layer would be deposited on this sublayer by the electron-beam physical vapor deposition (EB PVD) technique. The rationale was that the high quality and *fully stable alpha alumina layer* would prevent oxidation of the metallic substrate, which, as explained earlier, is the primary means by which TBC life is degraded. It is also important to note that discussions with the industry (both TBC manufacturers as well as engine companies) had shown that PVD was overwhelmingly favored over CVD techniques, largely because the system could easily be integrated with EB PVD systems that are already in use for depositing YSZ.

The alumina layer was planned to be essentially defect-free, without the presence of mixed oxides that normally exist in thermally grown TGOs. The rationale was that this high quality alumina sublayer would be highly resistant to the inward diffusion of oxygen. Yttrium (Y) doping would be considered because it has been shown to significantly reduce *grain-boundary* oxygen diffusion in alumina, the primary route for inward oxygen diffusion.

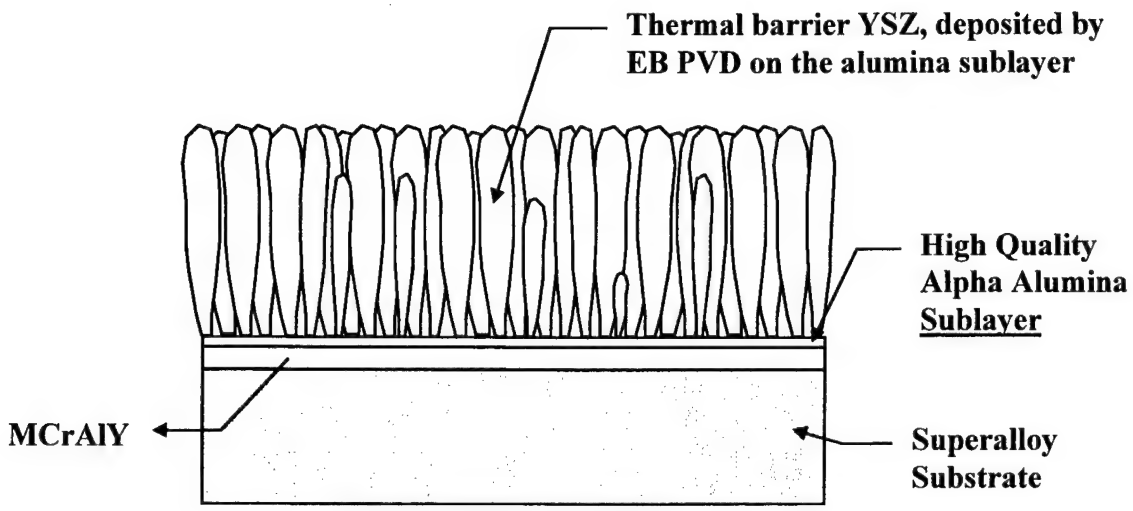

Figure 6. The approach of UES for the TBC system. It consists of a MCrAlY (more appropriately NiCoCrAlY) layer, followed by a 0.5–0.6 μm alumina sublayer. The alumina is deposited by the filtered cathodic arc technique. The thermal barrier YSZ layer (~100 μm thick) is deposited by EB PVD.

The technical work relied on a patented filtered cathodic arc deposition process [14,15] to deposit the alpha alumina sublayer at elevated temperatures (see Figure 7). This process provides high plasma ionization (>90%) compared to standard PVD processes (<20%). The multiply charged ions provide high reactivity of the plasma, thereby allowing very good bonding to the substrate. With high current densities (~ 4-5 A/cm^2) possible in the arc process, the percentage of neutral molecules can be reduced to less than 0.1%. The filtered arc source allows deposition of droplet-free coatings by deflecting the plasma flow along the curvilinear magnetic lines of force towards the substrate, while the droplets, having straight trajectories, are captured on the baffles. This advanced filter design provides practically droplet-free coating on large areas, ranging from about 250 mm in width to heights on the order of 300 mm to 2 m or more. The patented auxiliary anode assembly facilitates the generation of a uniform, high density plasma in which the part is immersed. Consequently, the process is much less sensitive to line-of-sight issues, as is the problem with standard sputtering and EB PVD techniques. Also, the high degree of ionization, combined with the plasma blanketing effect, permits deposition of extremely uniform coatings without roughness or ridges.

The vacuum arc cathode is also a theoretically unlimited electron emitter, thus providing an efficient source of high-density electron current. In this mode, it facilitates the generation of a uniform, highly conductive ionized gas even without the metal plasma. This is utilized for ion-cleaning the substrate before coating deposition.

2.1 THE ALUMINA SUBLAYER ARCHITECTURE

A few points are worthy of mention regarding the alpha alumina sublayer:

(i) It is not clear whether a 0.5-1 μm thickness of the alumina layer will be sufficient to drastically reduce oxidation of the superalloy, since a typical TGO thickness in Pt-Al based bond-coat system is about 5 μm. Some diffusion data for Al and O ions in alpha alumina are relevant here. Studies using radio-active tracers [16] indicate that the lattice diffusion in undoped alpha alumina is about 6 orders of magnitude smaller than grain boundary diffusion. Therefore, one anticipates that grain boundaries would be the primary path by which oxygen is carried through the alumina to the bond-coat.

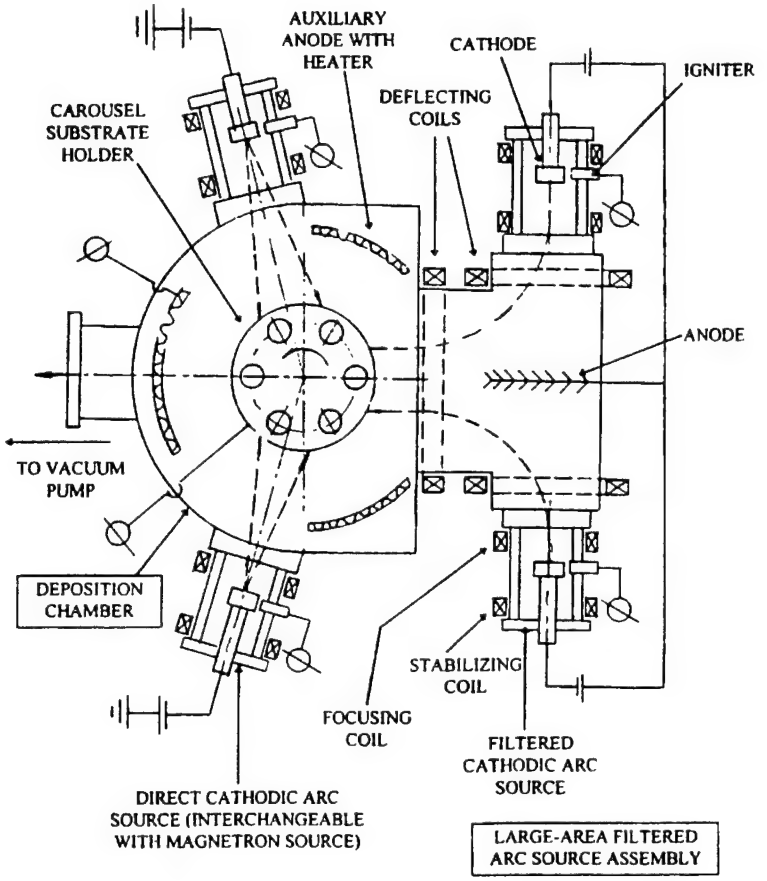

Figure 7. Sketch of the filtered cathodic arc deposition equipment at UES, Inc. showing the arrangements of the direct and filtered arc sources, auxiliary anode assembly, and substrate holder. The effective zone of deposition is approximately 15 inches in diameter and 16 inches high. The rotating carousal has 12 independent mounts and there are 4 layers.

One can also use the diffusion data to calculate the oxidation parabolic rate constant. This gives a parabolic rate constant of about 10^{-18} cm^2/sec at 1100°C, whereas the measured parabolic rate constant for alumina scale growth on a nickel base alloy substrate is about 10^{-13} cm^2/sec at the same temperature. This large difference suggests additional short circuit paths, mixed transition metal oxide formation, and defects in the alumina layer, during oxidation at 1100°C. The significant implication here is that if indeed a high quality alpha alumina layer can be deposited on the superalloy, then it may be possible to reduce the parabolic rate constant by as much as one to two orders of magnitude.

Given that a limited degree of oxidation of the metal will still occur, it becomes important to probe the mechanism of oxidation. There can be both an inward diffusion of oxygen through the cathodically coated alumina layer, as well as an outward diffusion of Al through that layer. These mechanisms would have important effects on delamination stresses and on the morphology of the metal-oxide interface.

(ii) The grain boundary diffusivity in reference [16] was observed to be as much as three orders of magnitude lower for an alpha alumina doped with 300 ppm Y as compared with

the undoped alumina. The Y^{3+} ions at the grain boundary were believed to have caused this reduced diffusivity. In reference [17], 6 wt.% Y_2O_3 reduced the sintering capability of CeO_2 by a factor of hundred, once again showing the large effect of Y^{3+} ions in reducing grain boundary diffusion. In references [18,19], the presence of Y in a superalloy was found to give rise to well adhering, flat scale of alumina under conditions where oxidation of those alloys without Y additions formed convoluted, non-adhering scales. The wrinkled scales were attributed to lateral growth of oxide resulting from oxide formation at grain boundaries by reaction with oxygen moving along the boundaries, with Al ions migrating through the bulk of the Al_2O_3 grains. This effect was reduced when Al bulk diffusion was reduced by addition of Y. In reference [20], Y^{3+} was shown to be an iso-electric donor in alpha alumina in spite of the same charge as Al^{3+}, and this behavior was attributed to the large size of the Y^{3+} ion. This donor effect was considered to be responsible for the reduction in sintering rate of Al_2O_3 doped with Y [21,22]. In the proposed work, we intended to take advantage of this effect, by introducing minute levels of Y during cathodic arc deposition of the alumina. It is important to note here that although Y has been added in the past to the bond-coat for oxide adhesion, there have been very limited attempts at introducing Y during alumina formation by a CVD process. The heavy element slows down the coating process, and has generally not been very successful. Consequently, the use of the cathodic arc deposition process offers significant advantage in reducing oxygen penetration through alumina. This approach may be considered as novel in the TBC development, with patent implications.

(iii) Another important issue is the oxidation of the metal underneath the alumina layer, since there will always be some diffusion of O through the alumina. The issue is whether the metal substrate needs to have high levels of Al (~50 atomic percent) to foster Al_2O_3 growth, in preference to nickel oxides, chromium oxides, or spinels. These latter oxides are fast growing, and their volumetric changes can have significant damaging influence on the integrity of the alumina coating. On the other hand, too high a level of Al in the superalloy or bond-coat renders them brittle.

Although a detailed oxidation study has not been performed, we can perhaps use thermodynamic data to shed some insight here. The Ellingham diagram shows that the partial pressure of oxygen that is in equilibrium with the alumina at 1100°C is only about 10^{-32} atmospheres. At this low partial pressure, only aluminum oxide can nucleate and grow, and not any transition metal oxide. The only other elements that will compete for the oxygen will be Y, Hf, etc. Past literature indicates that selective formation of such oxides below the outer oxide layer is extremely beneficial to oxide adhesion, since they tend to form pegs that hold the alumina to the metal [23]. Also, such pegs are barriers to the growth of delamination cracks. Therefore, as long as there is a reasonable supply of Al, (a) it is unlikely that mixed oxides will nucleate and grow below the alumina coating, and (b) Y or Hf in the metal will be of great benefit to oxide/metal adhesion. In other words, too high an Al level is not needed in the substrate below the alpha alumina layer.

3.0 EXPERIMENTAL PROCEDURE

The base material selected for the investigation was a MAR M-247 superalloy that was plasma coated at Chromalloy, New York, with 75–100 μm thick NiCoCrAlY coating. The nominal composition of the NiCoCrAlY was stated as: Co 19-25%, Cr 15-22.5%, Al 11-13%, Y 0.001–0.45%, Bal. Ni, all in wt.%. The coated coupons received Chromalloy's standard heat treatment, involving 4 hrs. at 1100°C in vacuum. The purpose of the heat treatment was presumably to stabilize the two-phase NiCoCrAlY microstructure. However, as will be shown later, this treatment did little to reduce the extent of bondcoat microstructure changes that occurred at temperatures of 1100°C and above.

The test coupons were of approximate size 20 mm x 12 mm x 3 mm. They were metallographically polished on the NiCoCrAlY side up to 1 μm diamond. These were then washed and cleaned, prior to being coated at UES with alumina using the filtered cathodic arc deposition system. The 1100 grade aluminum targets were used for the cathodic arc deposition. The depositions were conducted at high temperatures, in order to obtain the stable alpha-alumina phase. Because the existing filtered cathodic arc unit had capability only up to 450°C, a special tubular furnace was constructed with capability up to 1000°C. The sample was mounted inside the furnace, which was held horizontal to allow the impingement of Al and O_2 ions. This necessarily limited the coating to only one face of the sample. However, this limitation was considered sufficient for the Phase I program, since the real goal was to establish the feasibility of the highly stable alpha alumina film. It is important to note that the 1000°C capability is unique to any physical vapor deposition system, since the maximum capability of most systems is only about 850°C.

Prior to deposition of the alumina coating, the substrate was arc cleaned at the desired temperature. Next, a mixture of oxygen and argon gas (approximately in the ratio 80:20) was introduced into the chamber. The carrier argon gas was needed to minimize oxidation of the Al cathode, and thereby minimize instability of the arc. The substrate was RF biased, since prior research suggested that RF biasing was conducive to both improved coating/substrate adhesion, as well as the formation of high temperature phases. A total of approximately 25 coating runs were conducted, in order to establish robust conditions for the deposition of the highly stable alpha alumina phase.

Coating thickness was limited to 0.5–0.6 μm. This value was based on two considerations: (i) having a low enough thickness to reduce spalling of the alumina layer, since a smaller volume would necessarily possess less elastic energy might drive an interface crack, and (ii) having some level of thickness, to reduce oxygen penetration into the substrate and thereby reduce oxide growth. However, the thickness of 0.5–0.6 μm was just an initial estimate, and an optimum thickness would have to be obtained in a possible Phase II program.

In addition to coating the superalloy samples, small pieces of Si wafers were also coated. These latter samples were used to obtain a quick assessment of the alumina crystal structure using transmission electron microscopy (TEM). However, the final evaluation of the alumina crystal structure was always conducted on the NiCoCrAlY-coated superalloy substrates.

Two variations of the coating runs also were performed. In one case, a dilute dispersion of fine alpha alumina in distilled water (alumina particle size ranged between 50 nm and 300 nm) was spin coated on the substrates [24]. The rationale was that these alpha alumina particles would act as nucleation seeds, in that they would help to reduce the temperature at which alpha alumina coating could be obtained by the cathodic arc deposition process. It was felt that any lowering of the temperature for alpha alumina deposition would make the process much more technologically attractive. It is relevant to note here that diamond seeding had been found to be conducive to the formation of diamond film on SiC particles/whiskers [25].

In another variation, a high vacuum PVD process was utilized to deposit alumina that was doped with Fe. This method was once again attempted in order to reduce the temperature for alpha alumina deposition. The approach was considered because manufacturers of alpha alumina fibers take advantage of this doping to reduce the temperature for the formation of alpha alumina.

Other than these two variations, the bulk of the 25 coating runs involved the deposition of alumina using the filtered cathodic arc system. One set of alumina coated samples was further coated with YSZ using the EB PVD system at Chromalloy, New York.

Following alumina deposition, the coupons were characterized in terms of their microstructure, crystal structure, and oxidation behavior. The crystal structure of the alumina coating was determined using the glancing angle X-ray diffraction technique. This technique is fairly sensitive to thin films, since the incident X-ray beam is maintained at a constant value of only 3–5 degrees, so as to obtain maximum counts from the film compared to the substrate. The sample is also spun rapidly about an axis perpendicular to the film surface, and only 2-theta is varied during the X-ray scan. The results show that this technique is a simple and effective method for determining the crystal structure of thin alumina films. The crystal structure of the alumina coating was also confirmed using TEM. The procedure involved cutting a thin strip of the coupon parallel to the alumina face, and then mechanically grinding down from the metal side to approximately 0.1 mm thickness. Samples were then jet-electropolished in a solution of 20 ml perchloric acid and 180 ml glacial acetic acid at zero degree centigrade; the voltage was approximately 12 V and the current density was 1–2 mA/mm^2. The TEM samples were further thinned using an ion-milling apparatus, and then observed on a Hitachi TEM.

In addition to the above two techniques, we also experimented with the Raman scattering technique to determine the crystal structure of the alumina. The advantages of this technique are two-fold: (i) it has a spatial resolution of 1 μm, so that non-uniformity in crystal structure could be detected, and (ii) it can be used to determine the stress in the alumina film. Preliminary experiments indicated that the technique was only partially successful, with the Raman peaks often being masked by fluorescence associated with Cr in the subsurface region. Hence, the method was discontinued, although it may be used in the future for detecting stresses in the YSZ and alumina layers.

The alumina-coated coupons were sectioned and metallographically polished, and then examined using a scanning electron microscope (SEM). This procedure was conducted for the as-coated samples, as well as for samples that were exposed in air or vacuum at temperatures of 1100°C and above.

Mechanical characterization of the alumina coatings was conducted using a scratch tester. In this technique, a spherical diamond indenter is dragged on the coating at increasing indenter loads. The frictional resistance and acoustic emission (AE) signals are simultaneously monitored. The critical load (L_c) corresponding to the onset of significant AE signals is noted. However, this by itself is not sufficient to establish the onset of delamination. From the load L_c, the location of the scratch at which delamination occurs is estimated. Next, the scratch is observed using optical and SEM methods. A separate estimate is then made regarding the location at which delamination may have occurred. Based on a number of such observations, both from the AE signals and optical/SEM photographs, one can obtain a reasonable estimate of the load at which coating failure occurs. It is also important to note that there are two distinct failure modes. One is the delamination of the coating, and the other is transverse cracking of the coating. The latter may or may not be accompanied with delamination failure. Indeed, the alumina-seeded samples suggest that delamination failure did not occur even for fairly high loads.

The alumina coated samples were oxidized in air, under two different conditions: (i) 1150°C for 100 hours, and (ii) 1135°C for 100 hours. A companion sample without the alumina layer was also oxidized at 1135°C for 100 hours, in order to estimate the effect of the alumina coating on the oxidation behavior. The weights of the coupons were recorded before and after the oxidation treatment. However, because the alumina was coated on only one face of the coupons, the results of the weight loss/gain measurements were not very conclusive.

4.0 RESULTS

The cross-section of the NiCoCrAlY layer is illustrated in Figure 8, and it shows a two-phase microstructure, composed of light and dark phases. The light phase is a Cr-rich/Al-lean phase with the approximate composition: Ni-34.3, Co-28.6, Cr-27.7, Al-9.4, Y-0.01, all in at.%, as determined by the microprobe technique. This phase is the fcc gamma phase (and may contain the $L1_2$ gamma-prime

phase). The darker phase is rich in Al, and has the approximate atomic composition: Ni-44.2, Co-14.4, Cr-8.1, Al-33.3, and Y 0.04, all in atomic percent. This is the ordered beta (more appropriately B2) phase, and is the phase that provides the maximum oxidation resistance at 1000°C and above. The initial grain size was about 3 microns for each phase, but as will be shown later, the grain size increased to approximately 25 microns following exposure at 1135°C for 100 hours.

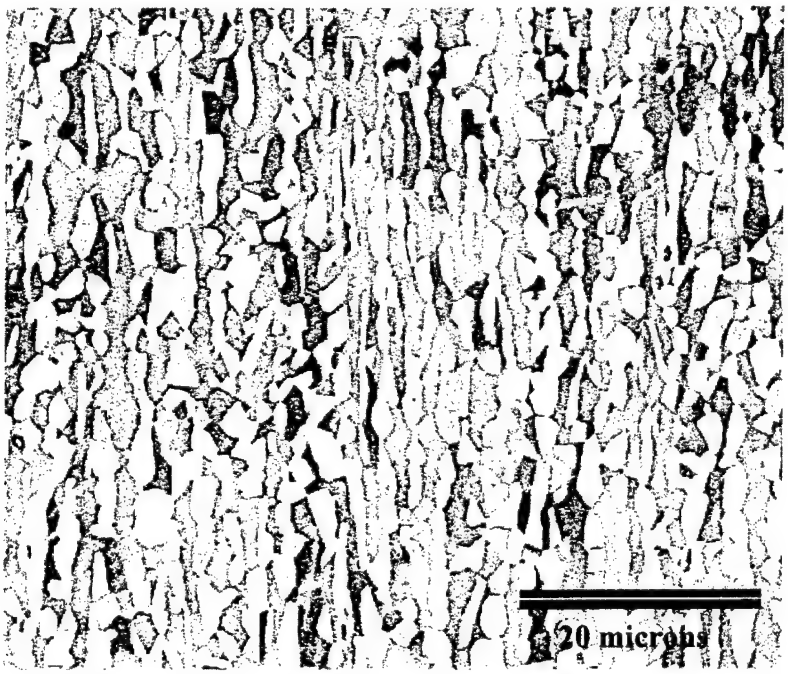

Figure 8. Microstructure through a section of the NiCoCrAlY bondcoat. The whiter phase is Cr rich (the disordered fcc gamma phase), whereas the darker grains are Al-rich (the B2 phase). The grains have a somewhat columnar morphology.

Figure 9a shows the cross section of sample 119 that was coated with alumina at 950°C. It is difficult to determine any microstructure of the alumina in the SEM image. Figures 9b and 9c show back scattered (BSD) images of a different sample, coated also at 950°C using a separate heater system. The defect structure at the NiCoCrAlY-superalloy interface is clearly visible in Figure 9b, as is the relatively fine structure of the two-phase alloy. Figure 9c shows a relatively smooth interface between the coating and the substrate, with the alumina coating appearing darker because of the lower atomic number of the constituents compared to the bondcoat. The EDAX analysis of the coating showed that the ratio of Al to O peak height was nearly identical to that for a polycrystalline alpha-alumina ceramic. Microprobe measurement of the alumina layer on a Si substrate showed stoichiometric composition. Thus, based on current results and those reported in the literature, the alumina stoichiometry appears to be fairly easily obtainable. It is the alpha phase that poses the most difficult challenge.

Auger analysis was conducted on a sample that was coated at 950°C. It indicated significant carbon contamination. It is likely that this carbon originated from hydrocarbon vapors in the vacuum chamber, although possible degassing from the heater system cannot be ruled out. The presence of carbon is detrimental to oxide adhesion, and efforts are under way to reduce this contamination to a minimum.

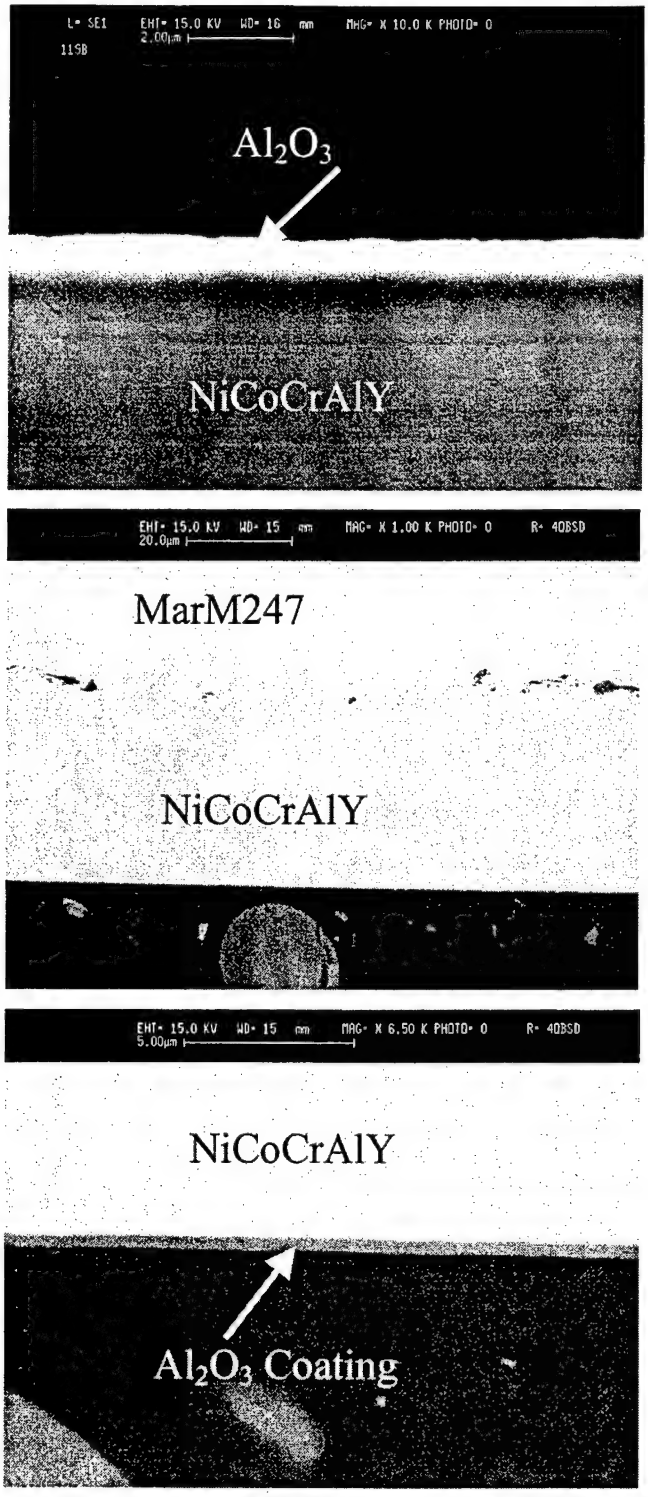

Figure 9. (a) As-coated sample, with the alumina layer appearing white. The darker region at the bottom is NiCoCrAlY. Coating thickness is approximately 0.5 microns. (b) A low magnification micrograph of a separate coated specimen, where the coating is at the bottom. The NiCoCrAlY microstructure is visible, and the pores define the original boundary between the EB PVD deposited NiCoCrAlY and the MarM247 superalloy substrate. (c) Higher magnification back scattered micrograph of Figure 9b. The darker thin band running horizontally in the middle of the picture is the alumina layer.

Figure 10a shows glancing angle X-ray diffraction data of the 950°C coated sample, illustrated in Figure 9a. Figure 10b is a glancing angle X-ray from some alpha alumina powder. Figure 10c shows X-ray diffraction data for the NiCoCrAlY, without the alumina coating. The important peaks to consider in Figure 10a (alumina coated sample) are the ones at approximately 3.49, 2.56, 1.74, and 1.60 Angstrom d-spacings. All these peaks correspond to alpha alumina, and are absent for the base NiCoCrAlY material. Figure 10d shows glancing angle X-ray for a sample that was coated at 850°C. In this case the alpha alumina peaks are missing. Together they indicate that alpha alumina can be obtained if deposition is conducted at 950°C and higher. To further confirm the detectability of alpha alumina, the sample of Figure 10d (coated at 850°C) was heat-treated in vacuum for 4 hours at 1150°C, to transform the alumina to the alpha alumina phase. Except for some cracks along the edges, the alumina coating was essentially intact. Figure 10e shows the glancing angle X-ray for this sample. The characteristic alpha alumina peaks can be observed once again for this sample. The same peaks were observed on samples oxidized in air for 100 hours. Thus these consistencies established the viability of using the simple glancing angle X-ray technique for detecting the formation of alpha alumina. Although not shown here, alpha alumina was also obtained at a substrate temperature of 925°C.

Alpha alumina was not obtained at lower substrate temperatures. Between 750°C and 850°C, only gamma alumina was obtained. At room temperature, the alumina phase was amorphous.

Figure 11 shows the selected area TEM diffraction pattern for sample 209 that was coated with alumina at 950°C. The rings with fine spots correspond to the coating, whereas the bigger spots correspond to the NiCoCrAlY. The d-spacings corresponding to the rings were obtained as 2.54, 2.17, 1.73, 1.52 1.24, and 1.05 Angstroms. These agree very well with the d-spacings for alpha alumina, namely 2.552, 2.165, 1.74, 1.52, 1.24, and 1.05 Angstroms. Thus, the TEM observations confirm the X-ray data, in that alpha alumina is obtainable if the deposition is conducted at 950°C.

Figure 12 shows the Raman spectra for sample 119, and that for an alpha-alumina powder (calibrating sample). The background slope for sample 119 is caused by flourescence associated with Cr in the sub-surface region. Nevertheless, the two small peaks (marked A and B) agree very well with those for the alpha-alumina standard. In some of the other samples, flouresecence appeared to completely mask all the alumina peaks, and hence this procedure was discontinued after initial trials.

Figure 13 shows the microstructure of a sample that was coated at 950°C, and then heat treated in a vacuum for 4 hours at 1150°C. The micrograph shows that the coating was perfectly intact. However, there was some coarsening of the NiCoCrAlY microstructure, as well as precipitation/coarsening of a finer phase in the disordered gamma phase.

Figure 14a shows the cross-sectional micrograph of sample number 121 that was coated at 950°C, then exposed in air at 1150°C for 100 hours. This is a fairly severe test of any coating without an outer zirconia layer. EDAX analysis showed that the dark outer layer at the bottom of the micrograph (approximate thickness 1.5–2.0 μm) was pure alumina. Since the original alumina coating was only 0.5 μm, it is clear that additional oxidation had occurred during the high temperature exposure. However, the original alumina is not distinguishable, and it is possible that the deposited layer may have delaminated over the 100 hours exposure. Figure 14b shows the microstructure of sample (number 119) after a separate oxidation run (1135°C for 100 hours). In this case, only a very thin oxide layer is observed (~0.3 μm), although it is not clear if this layer is a remnant of the deposited alpha alumina, or whether that alumina layer spalled and was replaced by a spalling fresh oxide layer. The sample weight loss was approximately 0.0011 grams. This may be compared with a companion NiCoCrAlY coated sample (without any alumina), for which the weight loss under the same conditions was 0.017 grams.

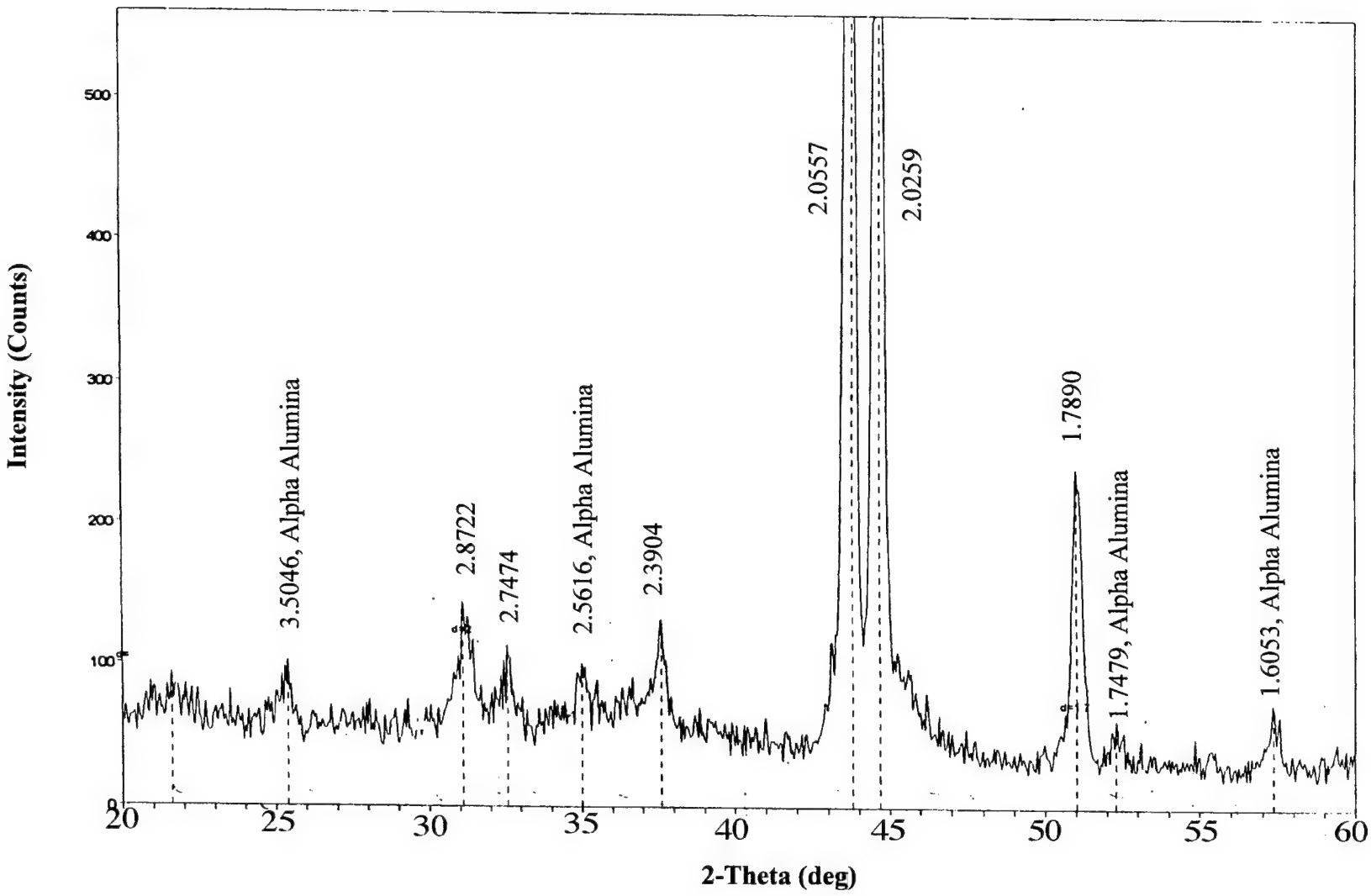

Figure 10. (a) Glancing angle X-ray diffraction of a sample coated at 950°C with alumina. The important peaks to note are the ones at approximately 3.50, 2.56, 1.74 and 1.60 Angstrom d-spacing. The three largest peaks at 2.06, 2.02, and 1.78 Angstroms correspond to the NiCoCrAlY layer.

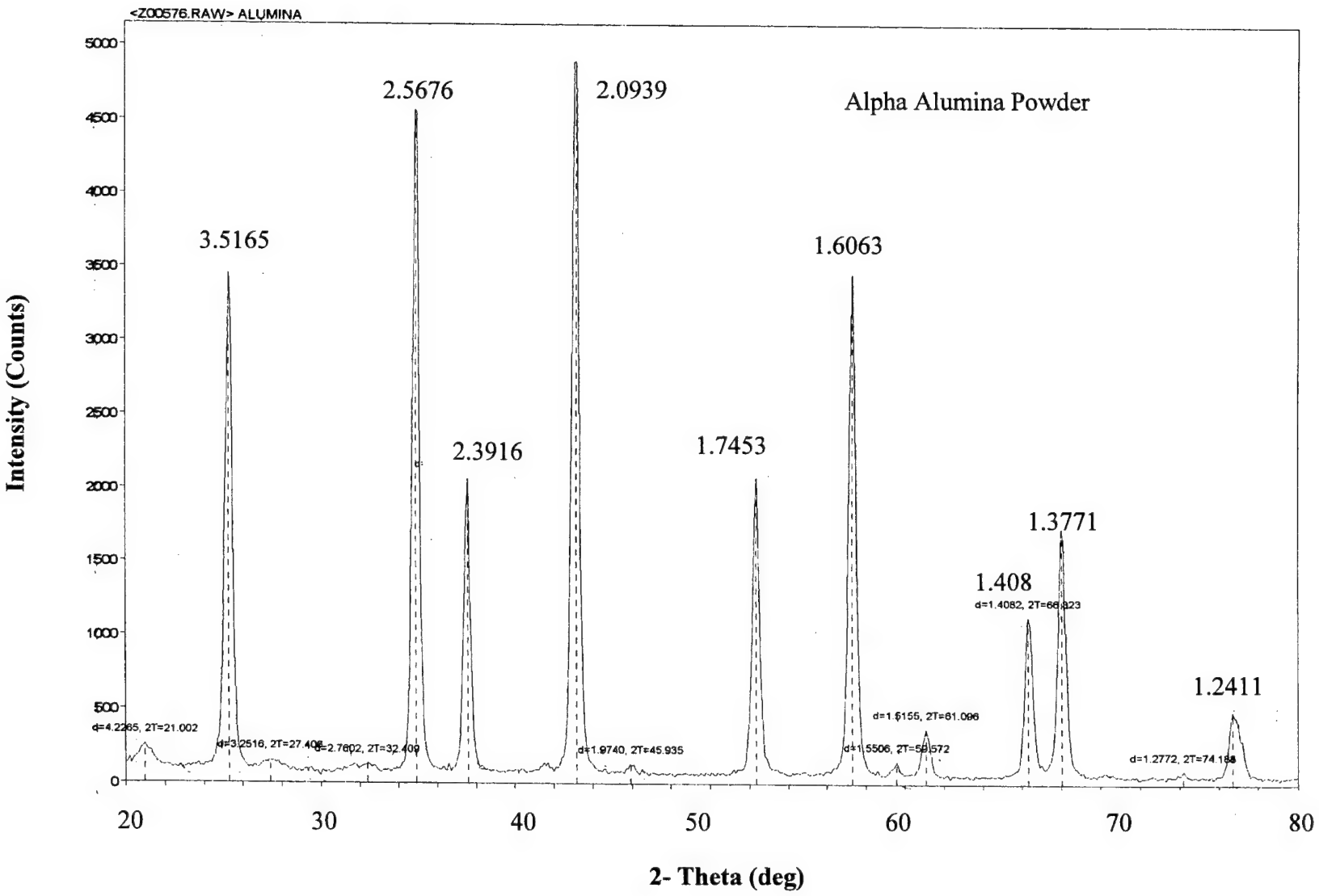

Figure 10. (b) Glancing angle for alpha alumina powder, showing typical peak positions.

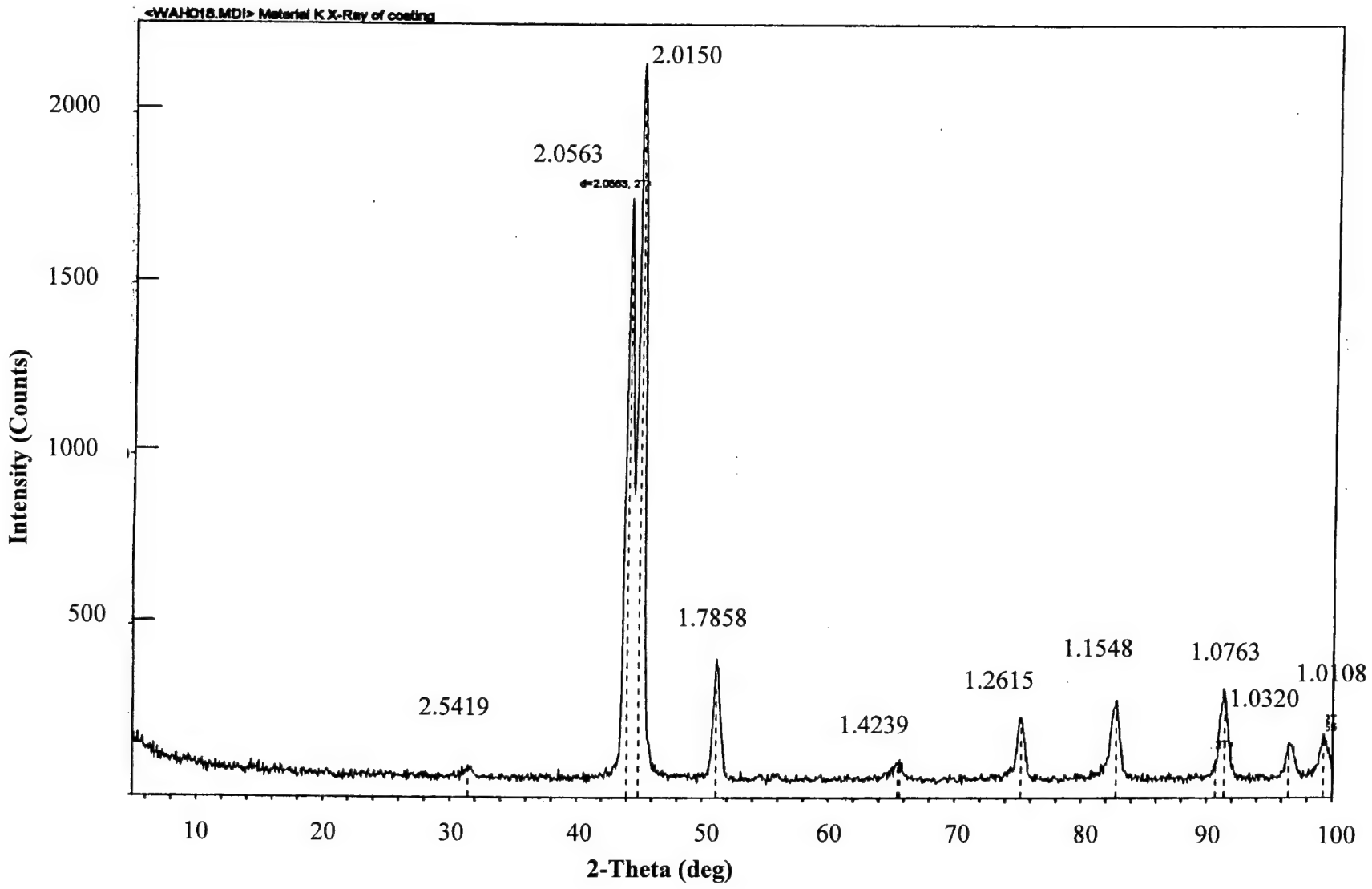

Figure 10. (c) X-ray diffraction of the NiCoCrAlY coating before any deposition.

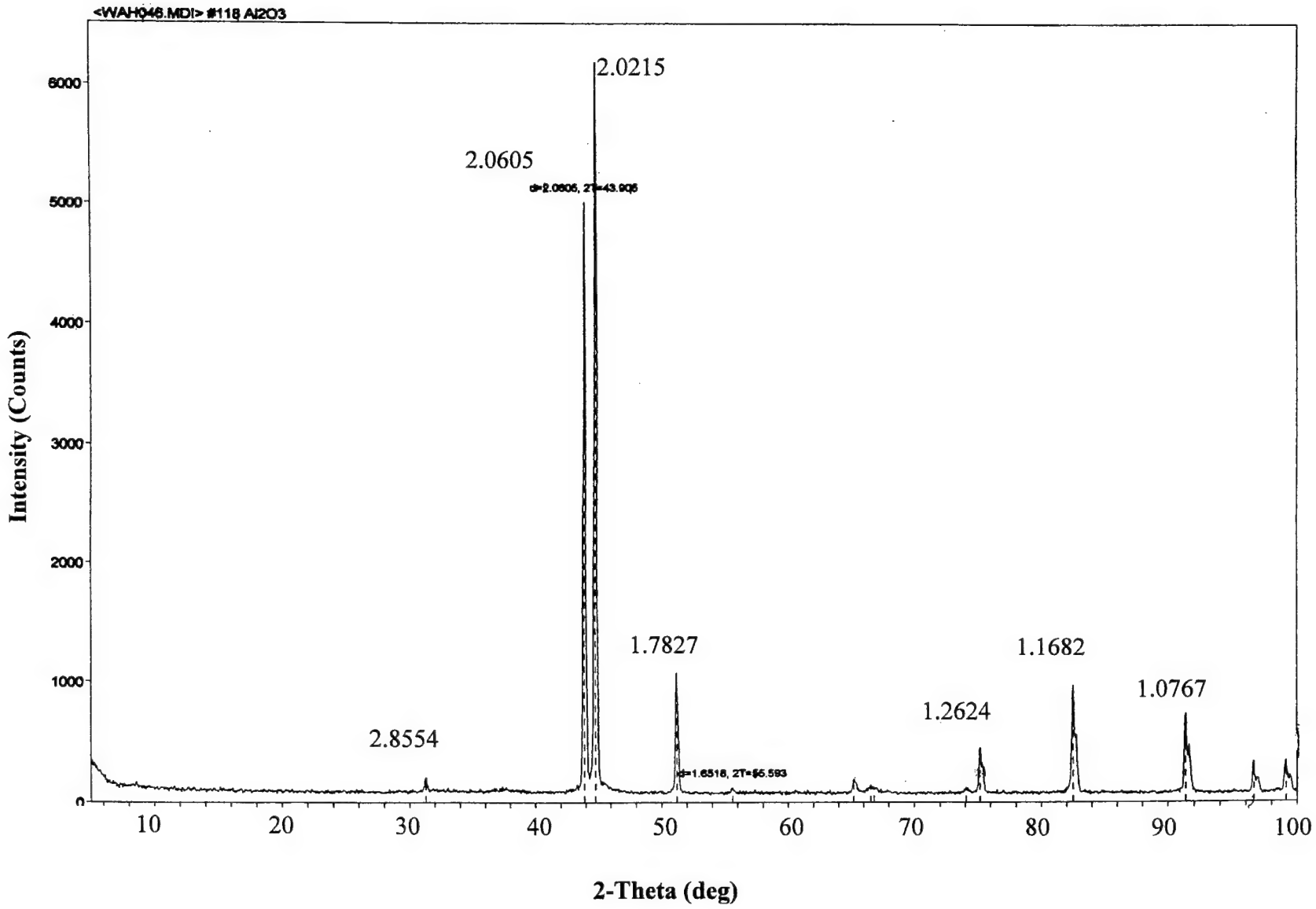

Figure 10. (d) Glancing angle X-ray diffraction of sample number 118 coated at 850°C. The characteristic alpha peaks are not visible.

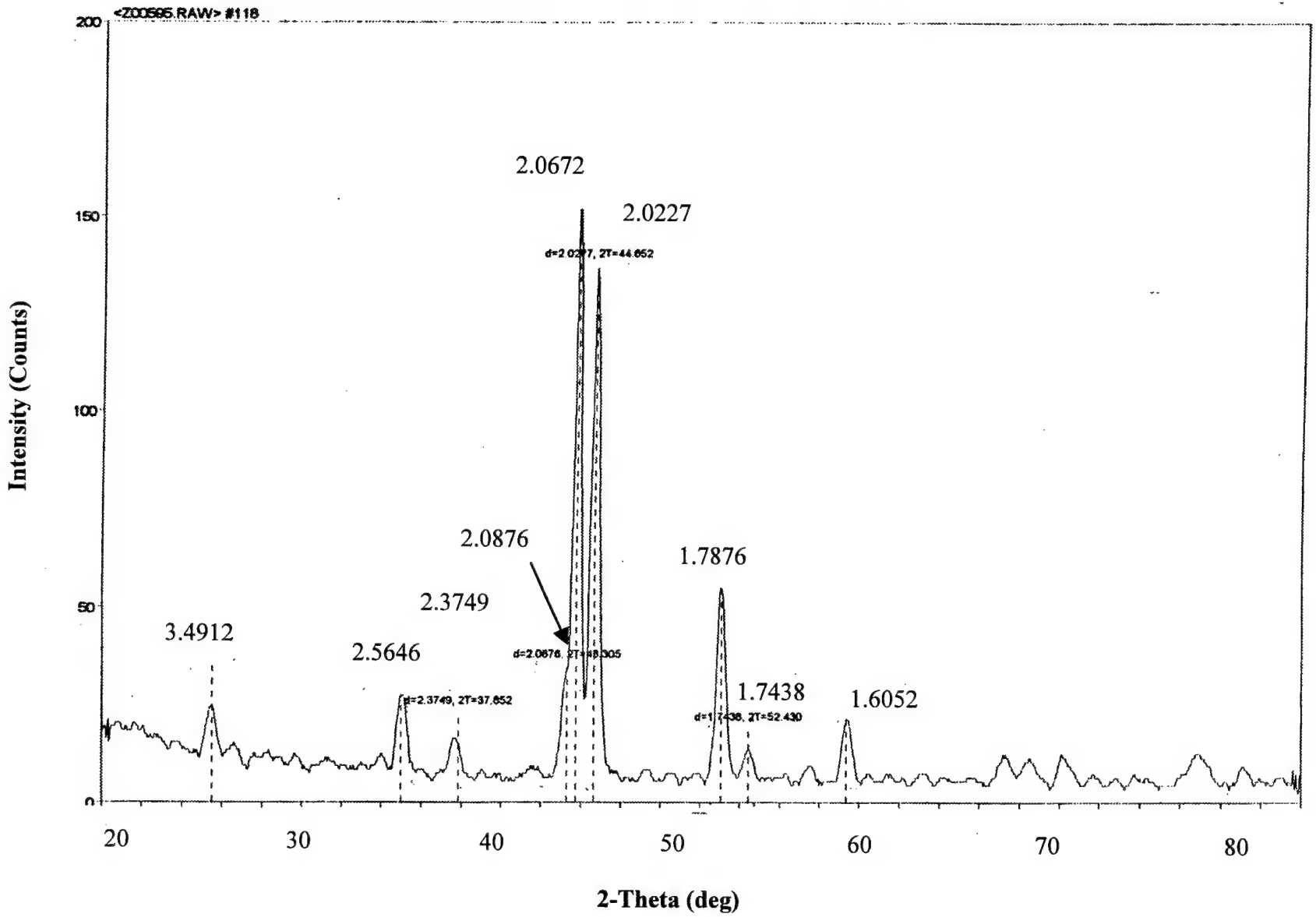

Figure 10. (e) Same sample as (d), after it was heat treated in vacuum at 1150°C for 4 hours. The alpha peaks reappear, consistent with transformation to alpha phase at the high temperature.

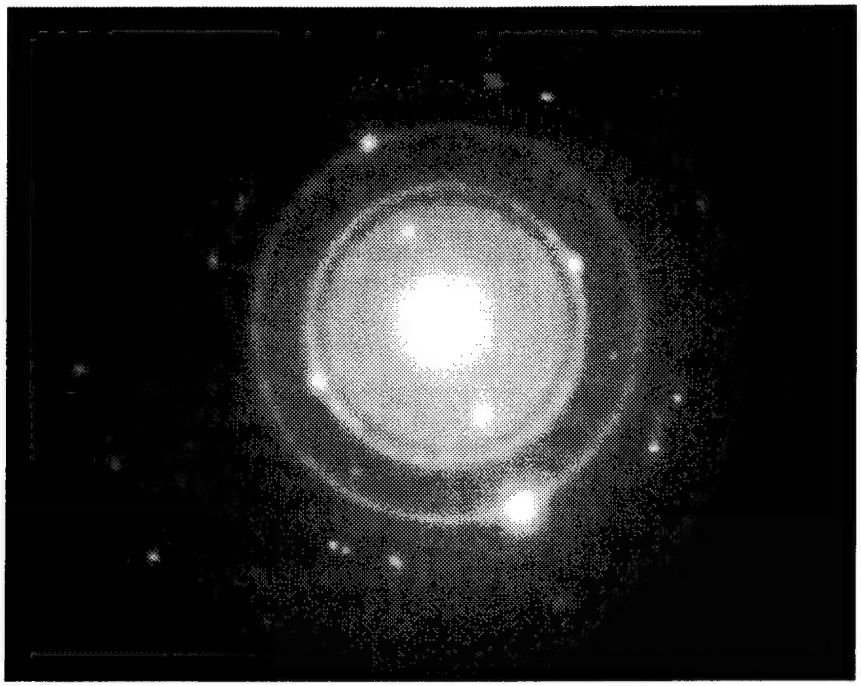

Figure 11. Selected area diffraction pattern of the alumina coating for sample 209, which was coated at 950°C. The rings with the fine spots correspond to the alumina layer, whereas the larger spots correspond to the underlying NiCoCrAlY layer. The d-spacing for the ring patterns confirm that the coating was alpha alumina.

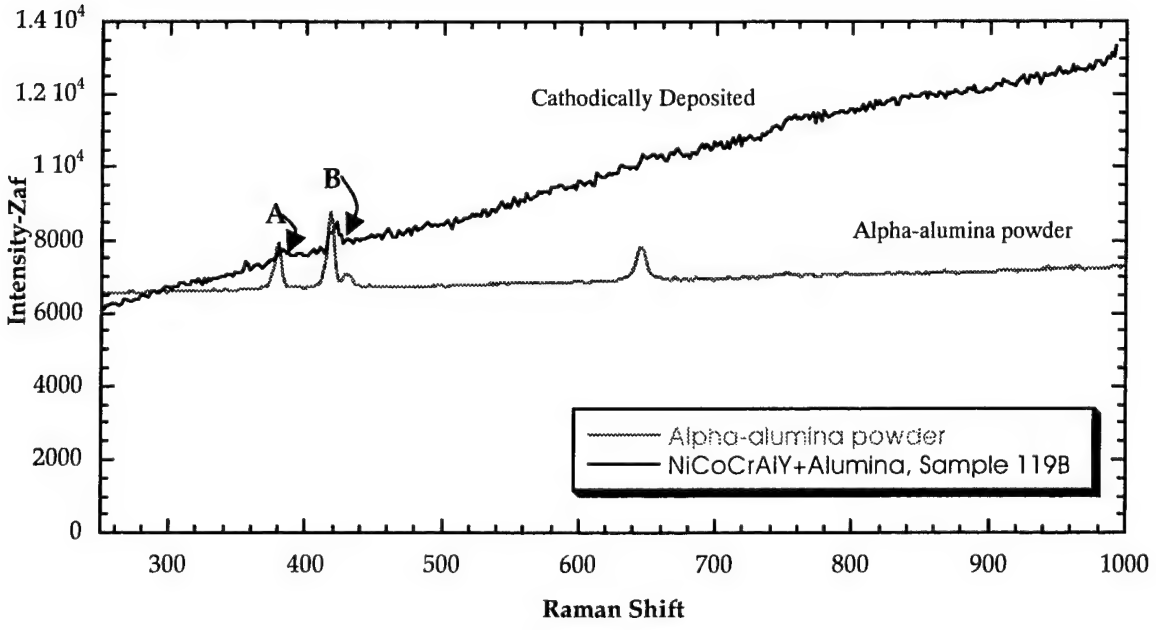

Figure 12. Raman spectra for sample 119 (cathodically coated with alumina at 950°C) and an alpha-alumina powder. The two peaks, marked A and B, do agree quite well with those of the alpha alumina powder.

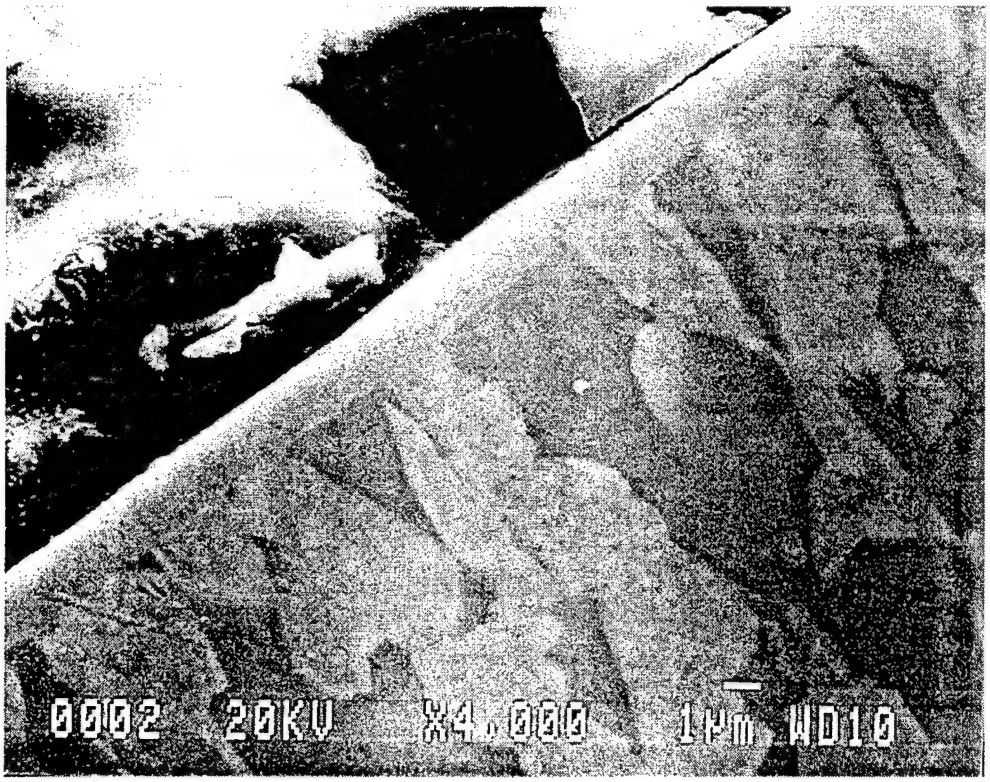

Figure 13. Microstructure of sample 119 that coated with alumina at 950°C, and then heat treated in vacuum at 1150°C for 4 hours. The alumina coating is perfectly intact.

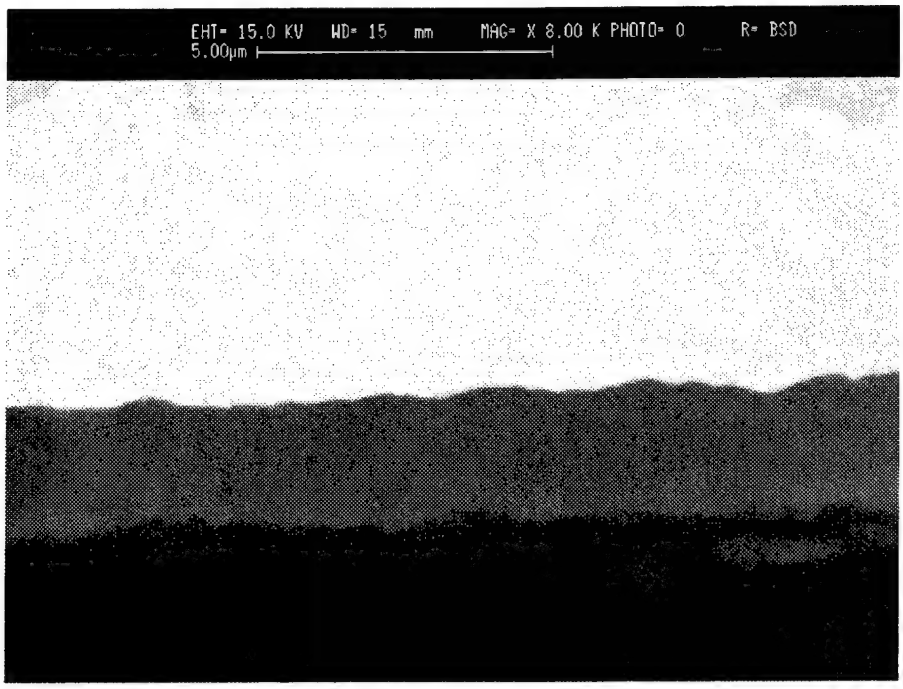

(a)

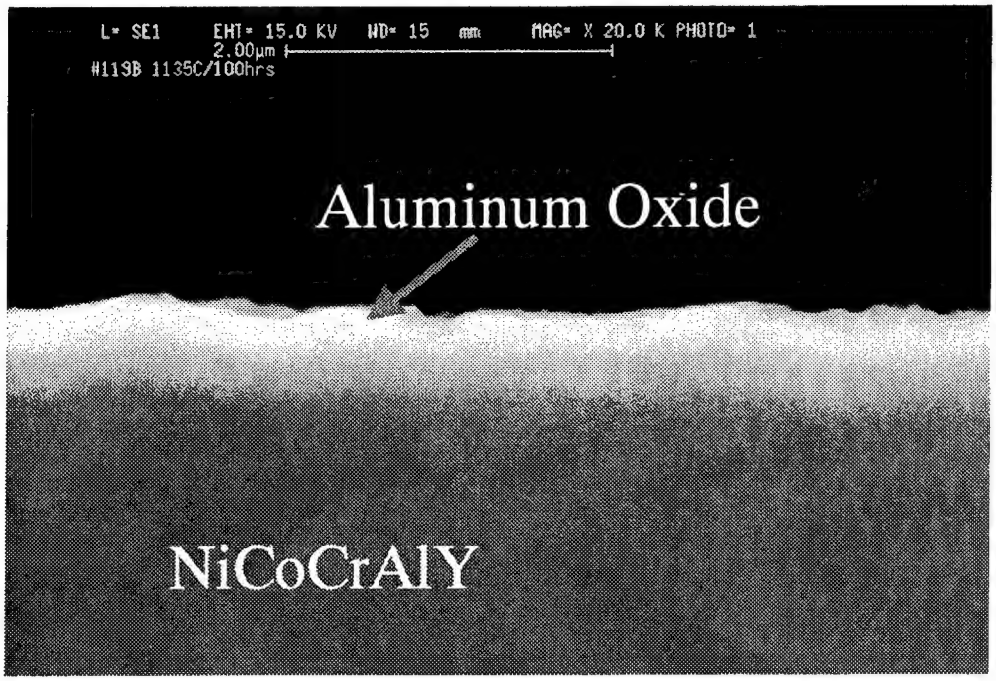

(b)

Figure 14. (a) Cross-sectional BSD image of sample 121, after exposure at 1150°C for 4 hours. This sample had been coated with alumina at approximately 950°C. The alumina layer appears as a darker horizontal band towards the bottom of the picture. (b) Sample 119 after a separate exposure at 1135°C for 100 hours. The top whitish band is alumina, based on EDAX analysis. However, its thickness is less than the original 0.5 micron thickness.

One of the problems faced in the program was significant microstructural changes in the NiCoCrAlY bond-coat, accompanied with surface rumpling. The former is illustrated in Figure 15a, and the latter in Figures 15b. The last figure clearly shows how surface rumpling has led to delamination of the coating. As indicated earlier, surface rumpling is extremely deleterious to coating integrity, and it appears that temperatures above 1100°C are unsuitable for the NiCoCrAlY bondcoat. In a recent paper [26], the mismatch between NiCoCrAlY and a single-crystal CMSX-4 alloy was estimated as approximately 0.3% at 1090°C. This is a significant strain level, and was indicated to be a major source of surface rippling of bond-coats on superalloy substrates [26].

The oxidation behavior was also studied for specimens that were not coated with alumina. In this case, the oxidation response was erratic. In one case, no oxide was observed, suggesting that the oxide may have spalled. In the second case, an oxide of approximately 4–4.5 μm was observed (see Figure 16), which was almost two times that for the alumina coated samples. The outer portion of the oxide contains Ni, Cr, and Al, suggesting the presence of the respective oxides, as well as spinels. The inner part of the oxide was simply alumina, and may have occurred because the local oxygen partial pressure drops significantly when a sizable oxide thickness is built up. Under very low partial pressure ($\sim 10^{-30}$ atmosphere), alumina and rare earth oxides would form in preference to oxides of Cr, Ni, or Co. The observed scale constituents are consistent with this description. However, if the layer spalled, then the entire oxidation process would repeat.

Thermal cycling was conducted between 200°C and 1177°C in air, both for an alumina coated sample (number 180) and for an alumina+YSZ coated sample (number 181-ZRO). The hold time at 1177°C was approximately 45 minutes, and the total cycle-time was approximately 65 minutes. Thermal cycling was conducted for only 25 cycles. Sample 180 showed many locations where the alumina had delaminated from the substrate, whereas sample 181-ZRO indicated that the coating was intact. Thus, as indicated earlier, thermal exposure of just the alumina coated material is much more severe than one with a YSZ top-coat. The YSZ coated sample was sectioned for metallographic examination. Unfortunately, we observed delamination of the coating from the substrate on either side of the cut plane. Detailed examination of the fracture path is still under investigation. A control platinum-aluminide+YSZ coated sample was also thermally cycled during this investigation. In this case, the sample was potted in an epoxy before it was sectioned, and it did not exhibit the extent of delamination that was observed in our alumina+YSZ coated sample. However, the polished section did indicate a number of locations where there was small-scale delamination between the TGO and the Pt-Al bond-coat.

Figures 17a and 17b are dark-field micrograph and diffraction pattern for sample 139Y that was seeded with alpha-alumina particles, and then coated with alumina using the cathodic deposition technique. The coating was applied at 850°C. Recall that in unseeded samples, this temperature resulted in the formation of gamma alumina rather than alpha alumina. Most of the rings in Figure 17b, particularly the strong ones, correspond to that of alpha alumina. Dark field images at different diffraction conditions indicated that the alpha alumina phase covered almost the entire region of the sample; i.e., the surface coverage was much larger than the initial coverage of alpha-alumina powder determined by high magnification SEM (see Figure 17c). While these results do not fully confirm that alpha alumina seeding may be beneficial to alpha-alumina formation at a lower temperature, the results are encouraging. Future efforts will attempt to confirm if this methodology of seeding is indeed beneficial in lowering the temperature for alpha alumina deposition.

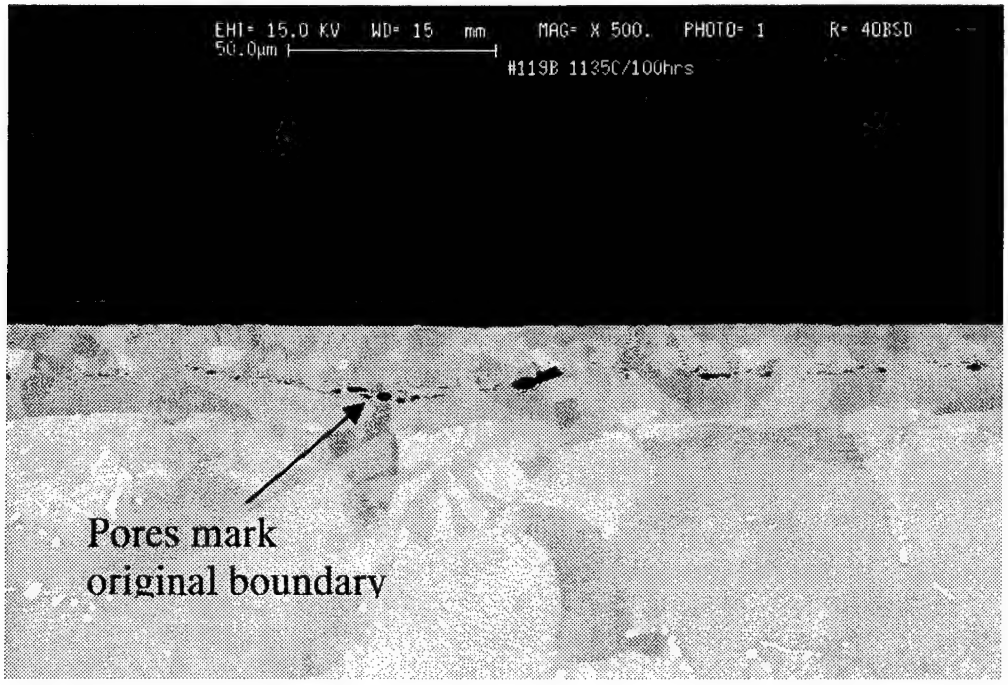

(a)

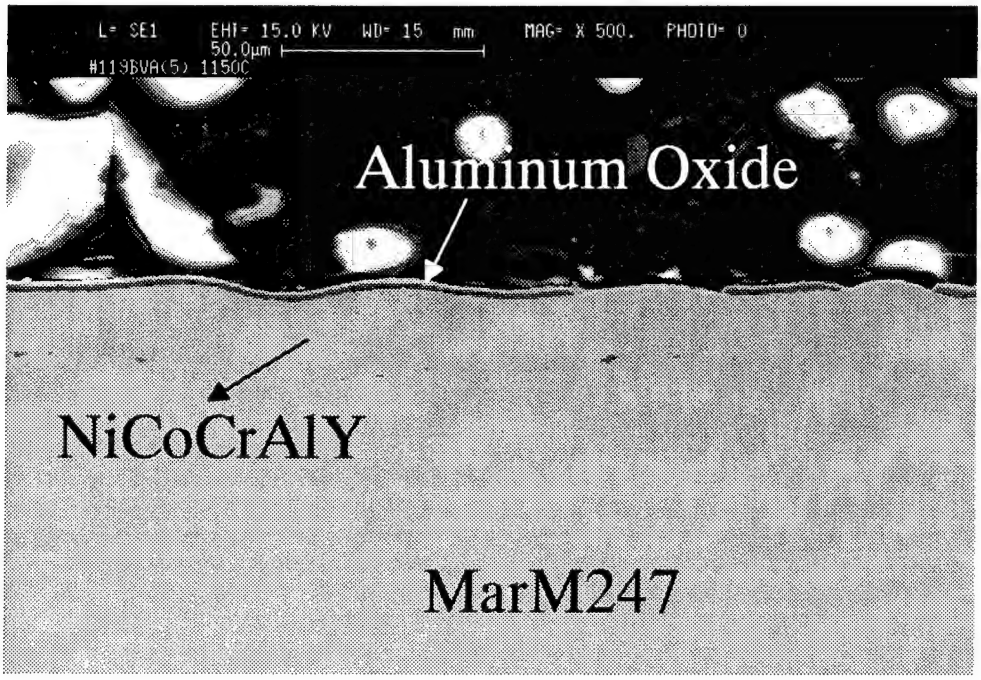

(b)

Figure 15. (a) Low magnification micrograph of sample number 119 exposed in air at 1135°C for 100 hours. Note the large grains (compare with Figure 8), and reactions with the superalloy (the large grains below the original pore boundary), indicating major microstructural changes of the NiCoCrAlY bondcoat. (b) Surface rumpling of the bondcoat for a sample exposed in air at 1150°C for 100 hours. Note how the oxide has spalled.

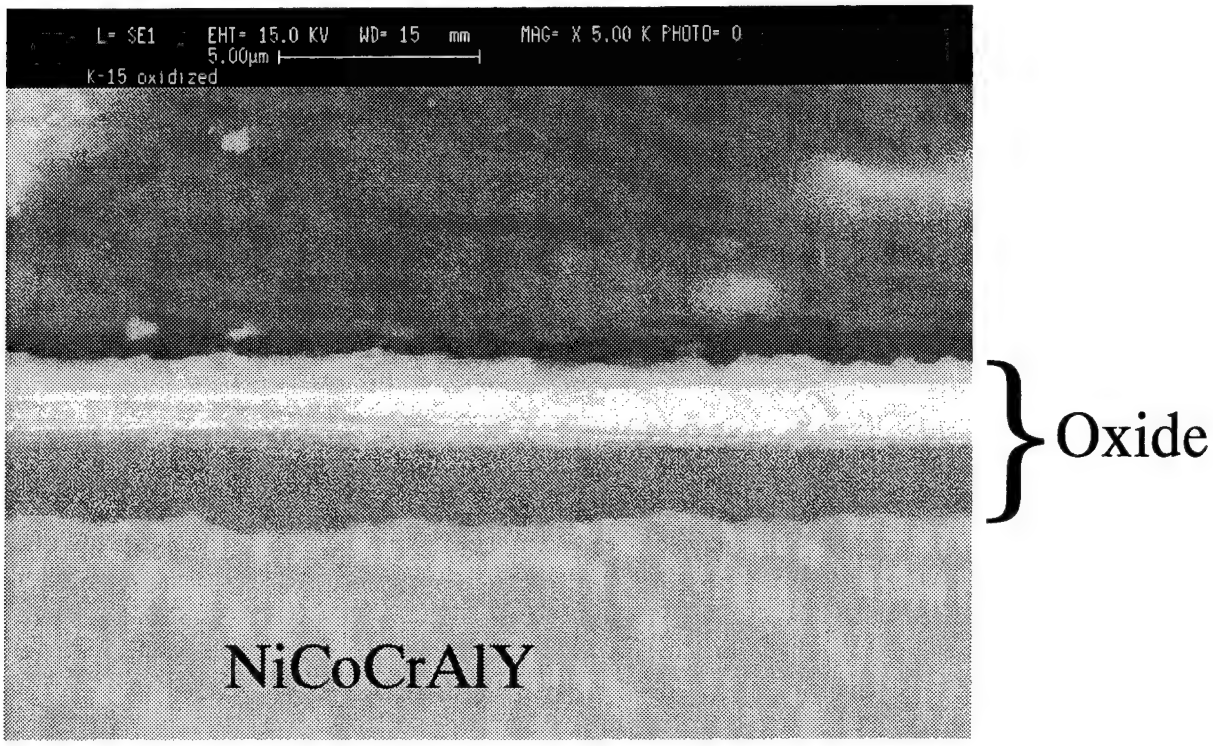

Figure 16. Oxide layer of a control sample (without alumina coating), oxidized in air at 1135°C for 100 hours. The total oxide thickness is approximately 4 microns. The outer bright spots on the oxide contain significant amounts of Ni and Cr, as determined by EDAX analysis. The oxide closer to the NiCoCrAly contains only Al and O, suggesting essentially pure alumina.

(a)

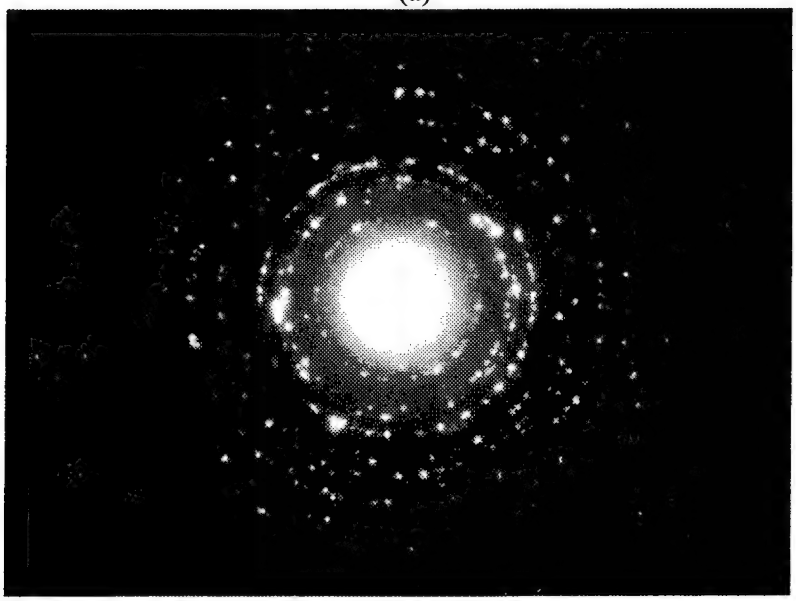

(b)

Figure 17. (a) Dark field and (b) diffraction micrographs for sample 139Y. This sample was initially seeded with fine alpha alumina particles, then cathodically coated with alumina at 850°C, which was lower than the standard temperature of 950°C. Most of the rings correspond to alpha alumina, suggesting that the alumina seeds may have facilitated formation of alpha alumina at a lower temperature.

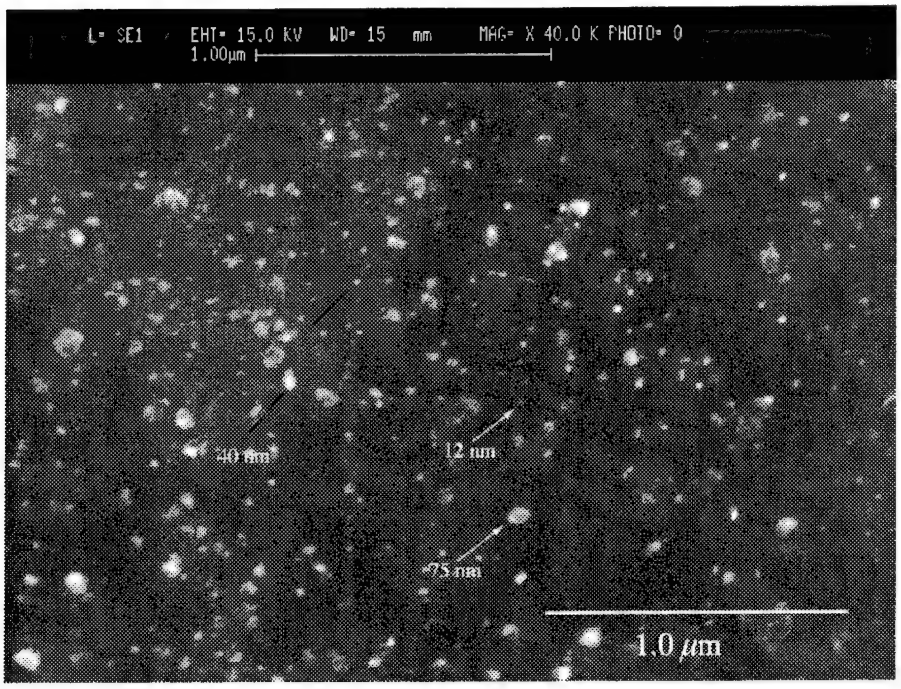

(c)

Figure 17. (c) High magnification SEM micrograph of the seeded sample prior to cathodic deposition of alumina. The white particles correspond to alumina seeds, and their size and surface coverage may be noted.

Figure 18a shows the scratch test result (using a 200 micron diameter diamond indenter) for the above 139Y sample. The change in slope in the load-displacement curve at point A was a result of slight slippage of the specimen, and was not due to any delamination. Indeed, the curve is linear up to the maximum load of approximately 60 N. The first major AE signal occurred at approximately 30 N. Observation of the specimen surface did not show any evidence of delamination. Rather, there was intermittent transverse cracking of the film. Figure 18b illustrates this transverse cracking at approximately 1 cm distance from the start point. The most important point to note is that while there is transverse cracking, there is no delamination of the film; this was observed all the way to the maximum load of 60 N. Thus, in spite of the presence of seeded particles, this coating showed excellent bonding characteristics.

The unseeded samples, coated at 950°C, also indicated a transverse cracking load between 30 and 45 N. In some case delamination was observed at a load of 50 N. The lowest delamination load was observed for a sample that was initially coated with yttria, then subsequently coated with alumina. In this case, delamination occurred at 45 N, and the scratch test results are shown in Figures 19a and 19b. It is important to note that delamination loads of 40 N and higher are considered quite good for hard coatings. Hence, the cathodic deposition system does appear to provide good bonding for alpha alumina.

5.0 DISCUSSION

The results indicate that one can routinely deposit alpha alumina using the cathodic deposition technique. This is a major accomplishment of the Phase I SBIR program. A principal requirement during deposition is that the substrate be held at a temperature of 925–950°C, or higher. At lower temperatures (i.e., 750°C and 850°C), only gamma alumina is obtained. This phase is not the most stable phase, and should be avoided.

The isothermal oxidation tests of the alumina coated samples were not very conclusive regarding the effectiveness of the alumina layer. There was cracking of the alumina layer as well as possible spallation. However, there are a few issues to consider here. First, there was significant instability of the NiCoCrAlY layer at temperatures of 1100°C and above. This was accompanied with surface rippling, which could create large tensile stresses in the alumina coating. Therefore, the bond-coat should be either stabilized by a long-term heat treatment in vacuum at temperatures above 1100°C, or it should be replaced by a more stable bond-coat, possibly one based on platinum aluminide. Second, we had observed carbon contamination of the alumina layer. This was likely due to hydrocarbon vapors in the vacuum chamber, and we have since made attempts to minimize this type of contamination. Third, the thin layer may not be sufficient to retard the ingress of oxygen, which can then lead to sub-surface oxidation. In our proposed approach, we had planned to incorporate yttria doping to combat the ingress of oxygen along alumina grain boundaries. However, a significant effort had to be spent in setting up robust condition for the routine deposition of alpha alumina. Consequently, we were able to make only one attempt, which involved prior deposition of a thin layer of yttria, followed by deposition of alumina. A homogenization heat treatment, followed by oxidation testing of this sample, has yet to be conducted. This data will provide confirmation of whether Y doping can indeed reduce oxidation substantially.

In an effort to understand the oxidation behavior of the alumina coated sample, we conducted 100-hour oxidation test at a lower temperature (1050°C), so as to reduce the effect of NiCoCrAlY instability. Weight gain/loss measurements indicated changes less than 0.001 grams. However, only one face of the sample was coated with alumina, so that weight change measurements may not provide much insight. Microstuctural characterization of this sample is still under way, and will be documented in the future.

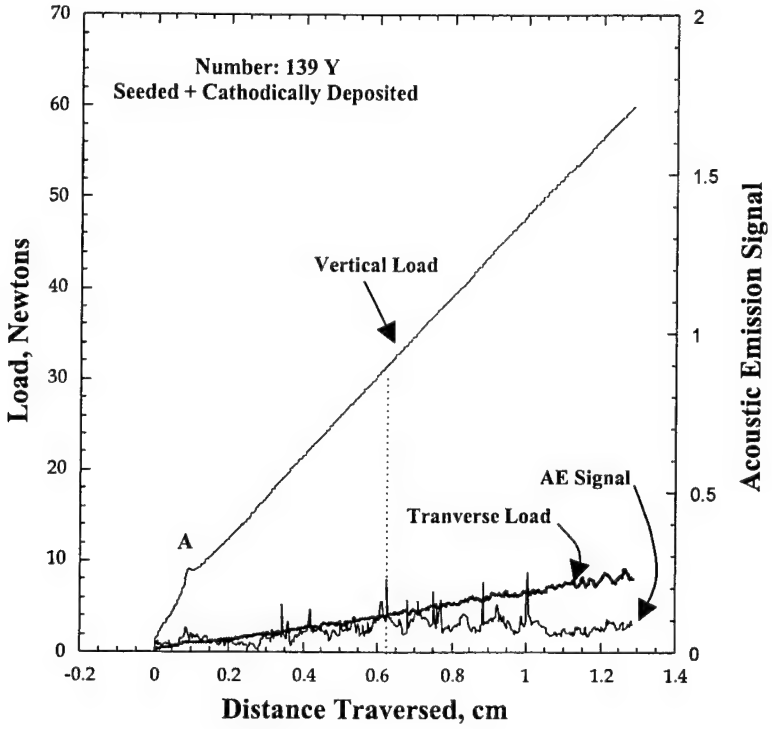

(a)

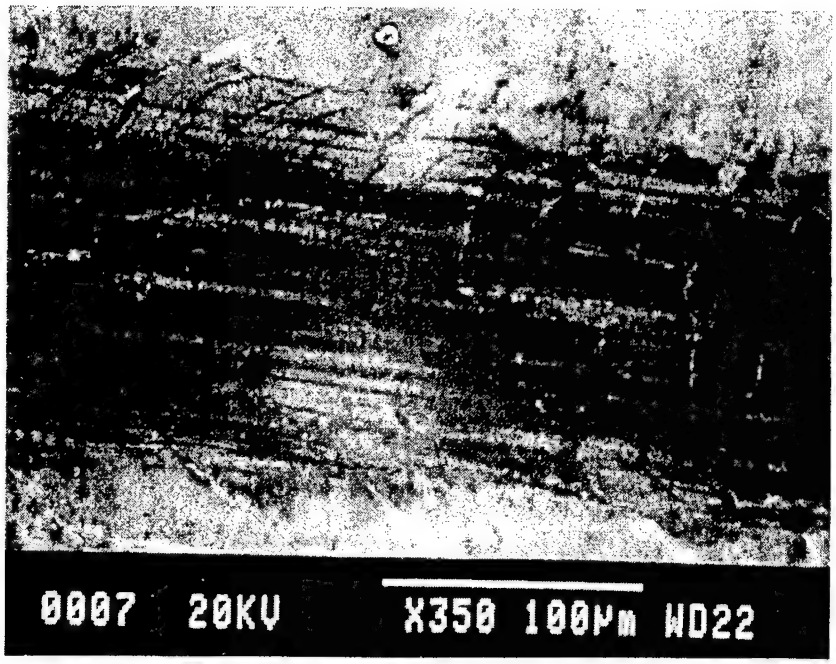

(b)

Figure 18. (a) Scratch test data for the above sample 139Y. The blimp at A occurred due to slippage, and not due to any delamination. (b) SEM micrograph of the scratch at a distance of approximately 1 cm from the initial point. The direction of indenter movement was towards the left. While there are transverse cracks, there is no evidence of delamination between the coating and the substrate.

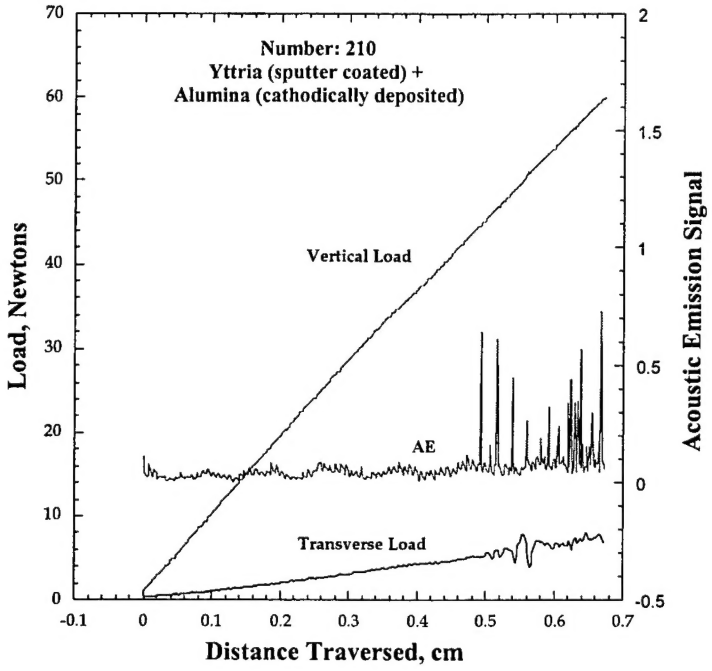

(a)

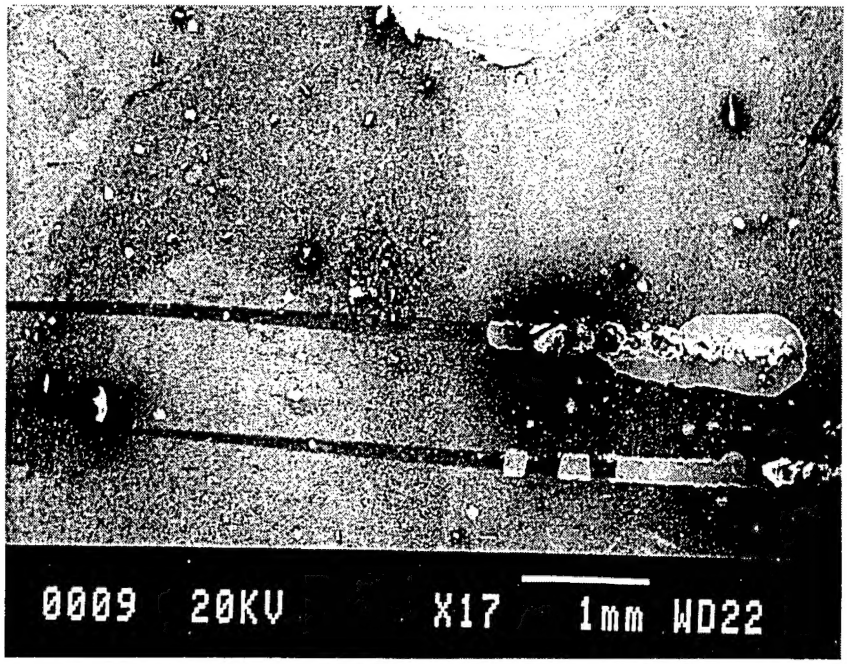

(b)

Figure 19. (a) Scratch test result for sample 210, which was initially sputter coated with a thin (<0.1 μm) layer of yttria, then cathodically coated with alumina at 950°C. (b) Scratch trace, and the location of delamination for the upper scratch coincided reasonably well with the mechanical test result (Fig. 19a).

The thermal cycling test result of an alumina-plus-YSZ coated sample (between 200°C and 1177°C) was encouraging. More tests of this nature need to be conducted, in order to obtain statistically significant data. Here too, the NiCoCrAlY layer should be stabilized above 1100°C, prior to coating with alumina and YSZ.

The scratch tests indicated reasonably good bonding between the alumina coating and the metallic substrate. Critical loads for delamination were 45 N and higher; in fact, in some cases no delamination was observed all the way up to the capacity of the instrument, namely 65 N. These loads compare favorably with data in the cutting tool literature, where critical loads for good coatings typically extend from 40 N to higher values. Thus, the cathodic deposition system is able to provide good interface bonds. Formulas are available that can reduce the raw critical load to a toughness value for the interface. These types of calculations will be performed in the future.

We have made one attempt to obtain alpha alumina at a lower temperature. The 850°C run on a seeded sample suggests that it may be possible to lower the deposition temperature, while still retaining the alpha alumina phase. However, additional experiments are necessary to confirm this finding. One interesting observation, regarding the use of seeded alumina on a Si single-crystal substrate, is worthy of mention here. In this case, the deposited alumina layer not only appeared to be of the alpha phase, but also the layer appeared to have a definite orientation relationship with the Si substrate. We do not yet have a rational explanation for this behavior. However, only one experiment was conducted, and we need to confirm the behavior using one more coating run.

While the seeding approach may appear to provide a weak interface, our scratch test results indicate that the nano-phase alpha alumina seed particles were not detrimental to adhesion. In fact, that sample appeared to have one of the highest interface adhesion. Thus, the seeding approach has merit, and needs to be evaluated in future work on advanced TBCs.

In this work we were unable to identify the mechanism of oxidation of the bond-coat with the top-layer of cathodically deposited alumina. As indicated earlier, the oxidation process may either be dominated by the ingress of oxygen through the alumina layer, or by the outflow of Al through that layer. Instabilities in the alloy, as well as cracking of the film, made it difficult for us to identify the dominant mechanism, although in one particular case it appeared that the outward Al flow was dominant. The literature data suggest that both mechanisms may be operative. Thus, in one case, radioactive tracers suggested that grain boundary transmission of oxygen made the main contribution to the growth of alpha alumina scales [27,28]. Conversely, a large part of the scale growth on NiAl at 1150°C was attributed to the outward transport of Al [29]. In the future, we plan to conduct oxidation tests at lower temperatures and shorter times, so that the mechanisms can be identified.

We were also unable to probe the effects of yttria doping on the oxidation behavior. As indicated earlier, a number of past studies suggest the beneficial effects of yttria in reducing diffusion rates of alumina. However, the level of yttria must be kept low, since high levels have been found to retard the formation of alpha alumina from metastable oxides [30]. For example, the transformation to alpha alumina more rapidly for yttria containing alloys [31], but less rapidly for yttrium implanted alloys [32]. Yttria also has been found to reduce the extent of convolution of the alumina scale [18]. This would be extremely beneficial in retaining the integrity of the cathodically deposited alpha alumina film. Therefore, considering all these advantages, doping with yttria needs to be considered seriously. We plan to conduct this in the future, by fabricating the cathode with an Al-Y alloy.

6.0 SUMMARY

In this work we have been able to routinely deposit alpha alumina on a NiCoCrAlY coated superalloy substrate. This has been the most significant achievement of the Phase I SBIR program.

Oxidation tests indicate that improvements are necessary for the current system to perform better than the best TBC system that is currently available. Factors that were responsible for poorer oxidation performance were identified, and these included instability and surface rippling of the NiCoCrAlY bond-coat, as well as carbon contamination of the alumina layer. Also, most of the oxidation tests were performed on just the alumina coated samples, which is a much more severe test for evaluating coating performance, compared to samples that have a YSZ top-coat. In the future, more thermal cycling tests on samples with a YSZ layer need to be conducted.

The alpha alumina seeding technique appears to have the potential to reduce the required deposition temperature for alpha alumina. However, this methodology needs to be verified by further experimentation.

7.0 REFERENCES

1. T.E. Strangman,"Thermal Barrier Coatings for Airfoils," Thin Solid Films, 127, p. 93-105 (1985).
2. J.T. Demasi et al., "TBC Life Prediction Model Development," P&W, NASA C.R.-182230 (1989).
3. J.T. DeMasi-Marcin and D.K. Gupta, "Protective Ccoatings in the Gas Turbine Engine," Surface Coat. Tech., *68/69,* 1 (1994).
4. R.V. Hillery, et al., "Coatings for High Temperature Structural Materials: Trends and Opportunities," National Materials Advisory Board Report, National Academy Press Washington, DC (1996).
5. S.M. Meier, D.M. Nissley, K.D. Sheffler, and T.A. Cruse, "Thermal Barrier Coating Life Prediction Model Development," Trans. ASME, 114, 258 (1992).
6. J. Doychak, J.L. Smialak, and T.E. Mitchell, "Transient Oxidation of Single Crystal Beta NiAl," Metall. Trans., 20A, p. 499 (1989).
7. R. Prescott, D.F. Mitchell, M.J. Graham, and J. Doychak, Corrosion Sc., Vol. 37, p. 1341 (1995).
8. I.G. Wright, B.A. Pint, W.Y. Lee, K.B. Alexander, and K. Prusner, Proceedings of Institute of Materials Conference on Surface Engineering, Edinburgh, UK (1997).
9. G.M. Newaz, Wayne State University, private communications.
10. V. Sergo, X. Wang, D. Clarke, and P.F. Becher, J. Am. Cer. Soc., 78, 2213 (1995).
11. J.A. Ahmad et al., "Design Tool for Oxidation and Thermal Protection Coatings," USAATCOM TR 96-D-11, Final Report to US Army Aviation Command, Oct. (1996).
12. W.Y. Lee, D.P. Stinton, C.C. Berndt, F. Erdogan, Y.D. Lee, and Z. Mustasin, "Concept of Functionally Graded Materials for Advanced Thermal Barrier Coating Applications," J. Am. Cer. Soc., Vol. 79, No. 12, p. 3003-3012 (1996).
13. J. Cheng, E.H. Jordan, B. Barber, and M. Gell, "Model to Predict Thermal Residual Stress and Failure of a TBC," presented at the 1998 Winter Meeting of the ASME, Anaheim, CA (Nov. 1998).
14. V.I. Gorokhovsky, U.S. Patents No. 5,380,421 and 5,435,900 (1995).
15. V.I. Gorokhovsky, Surface and Coatings Technology, Vol. 61, 108 (1993).
16. M. Le Gall, A.M. Huntz, B. Lesage, C. Monty, and J. Bernardini, "Self Diffusion in Alpha Alumina and Growth Rate of Alumina Scales Formed by Oxidation: Effects of Yttria Doping," J. Mat. Sci., p. 201-211 (1995).
17. M.A. Rahaman, R.E. Dutton, and S.L. Semiatin, "Effect of Solid Solution Additives on the Densification and Creep of Granular Ceramics," Acta Metall., 45, No. 7, p. 3017-3028 (1997).
18. F.A. Golightly, F.H. Scott, and G.C. Wood, "The Influence of Yttrium Additions on the Oxide Scale Adhesion to an Iron-Chromium-Aluminum Alloy," Oxid. of Metals, Vol. 10, p. 163-87 (1976).

19. F.A. Golightly, F.H. Scott, and G.C. Wood, "The Relationships Between Oxide Grain Morphology and Growth Mechanisms for Fe-Cr-Al and Fe-Cr-Al-Y Alloys," J. Electrochem. Soc., Vol. 126, p. 1035-42 (1979).
20. M.M. El-Aiat and F.A. Kroger, "Yttrium, an Isoelecrtronic Donor in Alpha Alumina," J. Am. Cer. Soc., Vol. 65, p. 28-283 (1982).
21. P. Nanni, C.T.H. Stoddart, and E.D. Hondros, "Grain Boundary Segregation and Sintering in Alumina," Mater. Chem., Vol. 1, p. 297-320 (1976).
22. B. Bender, D.B. Williams, and M.R. Notis, "Investigation of Grain Boundary Segregation in Ceramic Oxides by Analytical STEM," J. Am. Cer. Soc., Vol. 63, p. 542-546 (1980).
23. I.M. Allam, D.P. Whittle, and J. Stringer, "The Oxidation Behavior of CoCrAl Systems Containing Active Element Additions," Oxid. of Metals, Vol. 12, No. 1, p. 35-66 (1978).
24. M.A. Rahaman, University of Missouri at Rolla; we gratefully acknowledge his contributions in this activity.
25. P.A. Demkowicz, N.S. Bell, D.R. Gilbert, R. Singh, W.R. Drawl, and J.H. Adair, "Diamond-Coated SiC Whiskers," J. Am. Cer. Soc., Vol. 82, No. 4, p. 1079-81 (1999).
26. K. Fritscher, C. Leyens, and M. Peters, "Development of Low Expansion Bond-Coating for Ni-base Superalloys," Materials Sc. and Engr., Vol. A190, p. 253-258 (1995).
27. F.H. Scott, G.C. Wood, and J.Stringer, "The Influence of Alloying Elements on the Development and Maintenance of Protective Scales," Oxidation of Metals, Vol. 44, No. 1, p. 113-145 (1995).
28. K.P.R. Ready, J.L. Smialek, and R. Cooper, Oxidation of Metals, Vol. 17, p. 429 (1982).
29. E.W.A. Young and J.H.W. de Wit, Oxidation of Metals, Vol. 26, p. 351 (1986).
30. D.P. Moon, Mater. Sc. Tech., Vol. 5, p. 754 (1989).
31. W.J. Quaddekars, K. Schmidt, H. Grubmeier, and E. Wallura, Mater. High Temp., Vol. 10, p. 23 (1992).
32. J. Jedlinski and G. Borchardt, Proc. Symp. Oxide Films on Metals and Alloys, Vol. 92, Electrochem. Soc., p. 670 (1992).